NUMERICAL INVESTIGATION OF FLOW AROUND AN ISOLATED SPUR DIKE IN A CURVED CHANNEL

A THESIS SUBMITTED TO
THE GRADUATE SCHOOL OF NATURAL AND APPLIED SCIENCES
OF
MIDDLE EAST TECHNICAL UNIVERSITY

BY

EZGİ BUDAK

IN PARTIAL FULFILLMENT OF THE REQUIREMENTS
FOR
THE DEGREE OF MASTER OF SCIENCE
IN
CIVIL ENGINEERING

AUGUST 2017

Approval of the thesis:

NUMERICAL INVESTIGATION OF FLOW AROUND AN ISOLATED SPUR DIKE IN A CURVED CHANNEL

submitted by **EZGİ BUDAK** in partially fulfillment of the requirements for the degree of **Master of Science in Civil Engineering Department, Middle East Technical University** by,

Prof. Dr. Gülbin Dural Ünver
Dean, Graduate School of **Natural and Applied Sciences** _____

Prof. Dr. İsmail Özgür Yaman
Head of Department, **Civil Engineering** _____

Assoc. Prof. Dr. Mete Köken
Supervisor, **Civil Engineering Dept., METU** _____

Examining Committee Members:

Prof. Dr.İsmail Aydın
Civil Engineering Dept., METU _____

Assoc. Prof. Dr. Mete Köken
Civil Engineering Dept., METU _____

Prof. Dr. Zafer Bozkuş
Civil Engineering Dept., METU _____

Assoc. Prof. Dr. Yakup Darama
Civil Engineering Dept., Atılım University _____

Asst. Prof. Dr. Melih Çalamak
Civil Engineering Dept., TED University _____

Date: 10.08.2017

I hereby declare that all information in this document has been obtained and presented in accordance with academic rules and ethical conduct. I also declare that, as required by these rules and conduct, I have fully cited and referenced all material and results that are not original to this work.

Name, Last name : Ezgi Budak

Signature :

ABSTRACT

NUMERICAL INVESTIGATION OF FLOW AROUND AN ISOLATED SPUR DIKE IN A CURVED CHANNEL

Budak, Ezgi

M.S. in Department of Civil Engineering

Supervisor : Assoc. Prof. Dr. Mete Köken

August 2017 ; 63 pages

Secondary currents generated by meanders of the rivers cause scour along the outer bank of the rivers if the bed material is erodible. For this kind of rivers spur dikes are located along the outer reach where they regulate the flow and prevent erosion of the outer bank. In a highly curved channel several streamwise oriented vortices form within the bending section. However, presence of a spur dike causes the formation of some additional coherent structures such as horseshoe vortices and wake vortices. In fact, the interactions among these vortices and the secondary circulation results in a highly three dimensional complex flow field within the channel bend and around the spur dike. In order to be able to investigate the coherent structures and their interactions among each other eddy resolving method Detached Eddy Simulation was used in the present study. Different spur dike configurations were tested to understand the changes within the flow field and the coherent structures in a 180 degrees channel bend which has a flat bed. The results show that the presence of the

spur dike decreases the pressure root-mean-square fluctuations value and the spur dike orientation which lies in the flow direction is disadvantagous as it increases the bed shear stress considerably.

Keywords: Open channels, Coherent structures, Detached eddy simulation, Spur dike, Secondary flow, Curved channel

ÖZ

KURPLU BİR KANALIN DIŞ KENARINA YERLEŞTİRİLEN BİR MAHMUZ ETRAFINDA OLUŞAN AKIM ŞARTLARININ SAYISAL OLARAK INCELENMESİ

Budak, Ezgi

Yüksek Lisans, İnşaat Mühendisliği Bölümü

Tez Yöneticisi : Doç. Dr. Mete Köken

Ağustos 2017 ; 63 Sayfa

Menderesli nehirlerde kurpların yarattığı ikincil akımlar özellikle taban malzemesinin zayıf olduğu durumlarda nehir dış kenarı boyunca oyulmaya yol açmaktadır. Bu tür nehirlerde dış kenarda oluşan oyulmanın önlenebilmesi için kurbun oluştuğu bölgede bu kenara mahmuzlar yerleştirilmektedir. Keskin kavisli kanallarda akış yönündeki birçok girdap kurplu bölgede oluşur. Mahmuzlar, akımın bu bölgede düzenlenmesini ve nehir dış kenarının oyulmaya karşı korunmasını sağlamakla birlikte etraflarında atnalı vortekslerinin ve mahmuz gerisindeki vortekslerin oluşmasına sebep olmaktadır. Aslında bu vorteksler ile ikincil akımın birbiri ile etkileşmesi mahmuz etrafında kanal kurbuyla birlikte oldukça karmaşık üç boyutlu bir akımın oluşmasına yol açmaktadır. Organize akım yapılarının birbirleri ile olan etkileşimini inceleyebilmek için mevcut çalışmada bir vorteks çözümleme yönetimi olan ayrışan döngü benzetimi kullanılmıştır. Düz zeminli ve 180 dereceli

kurplu bir kanal içerisinde farklı mahmuz konfigürasyonları test edilerek her bir durumda organize akım yapılarının değişimi incelenmiştir. Sonuçlar mahmuzun eklenmesiyle tabandaki basınç değerlerinin düştüğünü ve akım yönünde uzanan mahmuzun taban zemin gerilmelerini arttırdığı için iyi olmadığını göstermiştir.

Anahtar Kelimeler: Açık kanal, Akım yapıları, Ayrışan döngü benzetimi, Mahmuz, İkincil akım, Eğimli kanal

To my family,

ACKNOWLEDGEMENTS

I would like to thank all the people who contributed to finish my thesis with their knowledge, help and supports in some way.

First and foremost, I would like to express my sincere gratitude to my advisor Assoc. Prof. Dr. Mete Köken for his continuous support, patience, motivation and immense knowledge. His guidance and understanding helped me in all the time of my study and I managed to write this thesis. I cannot imagine having a better advisor and mentor for my M.S. study.

I would also like to thank to the members of Hydromechanics Division of Civil Engineering Department at METU; Prof. Dr. Mustafa Göğüş, Prof. Dr. Nuray Tokyay, Prof. Dr. İsmail Aydın, Prof. Dr. A. Burcu Altan Sakarya, Prof. Dr. Zafer Bozkuş and Asst. Prof. Dr. Talia Ekin Tokyay Sinha for their vast knowledge. I learned a lot from them. Additionally, I would like to thank Necla Çankaya Lostar for her support. She was always helpful whenever I need. Besides, I would like to thank Assoc. Prof. Dr. Yakup Darama and Asst. Prof. Dr. Melih Çalamak for their interests in my work.

I would like to thank my colleagues for the duration of my entire work life at METU which was enjoyable thanks to them. I specially thank to Ezgi Köker for her endless support and helpfulness and valuable friendship. Ezgi, you were there whenever I need, I could not have enough patience without you. I also want to thank to Ali Ersin Dinçer for his valuable friendship. Ersin, your words always supported me with relieving and this provided less stressful study times during this process. Ezgi and Ersin I never forget the times we lived together. I feel very lucky to have your friendship. Another special thanks go to Ahmet Nazım Şahin for his intelligent ideas and valuable information that is very important in life time. In this process, you

always helped for raising me up when I fell down. I also want to thank Emre Haspolat. Emre, I had very enjoyable times thanks to you. You always made me smile with your ability to imitate and your funny memories.

Special mention goes to Tuğçe Yıldırım, Kutay Yılmaz, Serkan Gökmener and Abiddin Berhan Melek for their advices, helpfulness and friendship.

Also, I would like to thank my long-life friends. Very special thanks go to Merve Özen. Merve, I really could not write this thesis without you. You raised me up when I thought I cannot manage to make it and with your support I was able to progress in my study. Selen Öcal and Duygu Atasoy, I also want to thank you for your support in this process. Girls, I will always feel very lucky to have you in all through my life.

Merve Bilgin and Sinan Arslan, your friendship will always be precious even our cities are far away from each other. I always felt your support. I am very happy to meet you; your friendships are very valuable for me. Another special thanks go to Irmak Ünal. Irmak, you were always helpful and supporter during this process and you made me laugh even I was very miserable.

I also would like to thank to Hüseyin Çötel. Hüseyin, I was able to progress with your support although you joined my life not long ago. In this process, you supported me with your understanding, patience and love. I am very grateful to meet you.

Lastly but not leastly, I would like to express my deepest gratitude to my family for their endless understanding, support and love. My parents Asya Budak and Kenan Budak, my brother Deyiş Budak, my new sister Funda Budak and my lovely nephew Derin Budak, you have been always there as a continual source of support. I cannot imagine my life without you. I want to dedicate this thesis to you.

TABLE OF CONTENTS

ABSTRACT v

ÖZ vii

ACKNOWLEDGEMENTS x

TABLE OF CONTENTS xii

LIST OF FIGURES xiv

LIST OF SYMBOLS xviii

LIST OF ABBREVIATIONS xx

1. INTRODUCTION 1

1.1 Background 1

1.2 Literature Review 5

1.2.1 Studies related with Curved Channels 5

1.2.2 Studies related with Spur-dikes 8

1.3 Scope of the Study 12

1.4 Thesis Organization 12

2. NUMERICAL MODEL 13

2.1 Spalart-Allmaras One Equation Model 13

2.2 Spalart-Allmaras based DES model 15

2.3 Main Parameters, Computational Domain and Mesh 15

2.4 Boundary Conditions 18

3. ANALYSIS OF THE MEAN AND INSTANTANEOUS FLOW STRUCTURES IN THE CURVED CHANNEL WITHOUT SPUR DIKE 21

3.1 Grid Dependence Study 21

3.2 Description of the Main Vortical Structures in the Mean Flow 22

3.3 Description of the Seperated Shear Layers and the Turbulence Kinetic Energy Distribution 26

3.4 Pressure RMS Fluctuations and the Shear Stress Distributions 30

4. ANALYSIS OF THE MEAN FLOW STRUCTURES IN THE CURVED CHANNEL WITH SPUR DIKE 35

4.1 Description of the Main Vortical Structures in the Mean Flow 35

4.2 Description of the Seperated Shear Layers and the Turbulence Kinetic Energy Distribution 43

4.3 Pressure RMS Fluctuations and the Shear Stress Distributions 48

5. CONCLUSIONS 57

5.1 Summary and Conclusions 57

5.2 Future Works 59

REFERENCES 61

LIST OF FIGURES

FIGURES

Figure 1-1 The formation of the meanders ("GCSE Rivers Revision - The Middle Course," n.d.) 2

Figure 1-2 Typical spur dike in Hiji River in Japan ("Shallow Flow Visualization around a Single Groyne," 2007) 3

Figure 1-3 Sketch of the main coherent structures and physical phenomena present around an isolated spur dike (Koken & Constantinescu, 2008a) 9

Figure 1-4 Definition sketch (Shafaie et al., 2008) 10

Figure 2-1 General sketch of the model 16

Figure 2-2 Boundary conditions of Flow 3D simulation (P: pressure condition, W: wall condition, S: symmetry condition) 17

Figure 2-3 One Flow 3D solution 18

Figure 3-1 Non-dimensional mean streamwise vorticity distributions and corresponding streamline patterns at section D60 at a) finer mesh size case, b) coarser mesh size case 22

Figure 3-2 Three dimensional visualization of the vortical structure of the mean flow using the Q criterion 23

Figure 3-3 Three dimensional visualization of the vortical structure of the instantaneous flow using the Q criterion 24

Figure 3-4 Mean streamline patterns at sections a)P1, b)D0, c)D30, d)D60, e)D90, and f)D120 25

Figure 3-5 Mean streamwise vorticity distributions at sections a)P1, b)D0, c)D30, d)D60, e)D90, and f)D120 25

Figure 3-6 Mean streamwise velocity distributions at sections a)P1, b)D0, c)D30, d)D60, e)D90, and f)D120 26

Figure 3-7 Two dimensional streamline patterns (left), mean streamwise velocity contours, u_s/U (middle) and mean out-of plane vorticity contours, $\omega_z D/U$ (right) on horizontal planes at the level of a) 0.1D; b) 0.5D; c) 0.9D from the channel bed 27

Figure 3-8 Mean out-of plane vorticity, $\omega_z D/U$ contours for instantaneous flow at the level of a) 0.1D; b) 0.5D; c) 0.9D from the channel bed 28

Figure 3-9 Distribution of turbulent kinetic energy for the mean at the level of a) 0.1D; b) 0.5D; c) 0.9D from the channel bed..... 30

Figure 3-10 Distribution of the pressure RMS fluctuations, $p'p'/\rho U2$ a) on the channel bed, b) on the outer bank and c) on the inner bank..... 32

Figure 3-11 Position of the ζ value 32

Figure 3-12 Non-dimensional shear stress distributions, $\tau_w/\rho V^2$, a) on the channel bed, b) on the outer bank, c) on the inner bank..... 34

Figure 4-1 Three dimensional visualization of the vortical structure of the mean flow using the Q criterion a)at the whole channel, b)around the spur dike in case-S45 37

Figure 4-2 Three dimensional visualization of the vortical structure of the mean flow using the Q criterion a)at the whole channel, b)around the spur dike in case-S90 37

Figure 4-3 Three dimensional visualization of the vortical structure of the mean flow using the Q criterion a)at the whole channel, b)around the spur dike in case-S135 .. 38

Figure 4-4 Streamline patterns at sections a)P1, b)D0, c)D30, d)D60, e)D90, and f)D120 in case-S45 39

Figure 4-5 Streamline patterns at sections a)P1, b)D0, c)D30, d)D60, e)D90, and f)D120 in case-S90 40

Figure 4-6 Streamline patterns at sections a)P1, b)D0, c)D30, d)D60, e)D90, and f)D120 in case-S135 40

Figure 4-7 Non-dimensional mean streamwise vorticity distributions at sections a)P1, b)D0, c)D30, d)D60, e)D90, and f)D120 in case-S45 41

Figure 4-8 Non-dimensional mean streamwise vorticity distributions at sections a)P1, b)D0, c)D30, d)D60, e)D90, and f)D120 in case-S90 41

Figure 4-9 Non-dimensional mean streamwise vorticity distributions at sections a)P1, b)D0, c)D30, d)D60, e)D90, and f)D120 in case-S135 42

Figure 4-10 Non-dimensional mean streamwise velocity distributions at sections a)P1, b)D0, c)D30, d)D60, e)D90, and f)D120 in case-S45 42

Figure 4-11 Non-dimensional mean streamwise velocity distributions at sections a)P1, b)D0, c)D30, d)D60, e)D90, and f)D120 in case-S90 43

Figure 4-12 Non-dimensional mean streamwise velocity distributions at sections a)P1, b)D0, c)D30, d)D60, e)D90, and f)D120 in case-S135 43

Figure 4-13 (a) Two dimensional streamline patterns (left), mean streamwise velocity contours, u_s/U (middle) and mean out-of plane vorticity contours, $\omega_z D/U$ (right) on horizontal planes at the level of a) 0.1D; b) 0.5D; c) 0.9D from the channel bed in case-S45 45

Figure 4-14 Two dimensional streamline patterns (left), mean streamwise velocity contours, u_s/U (middle) and mean out-of plane vorticity contours, $\omega_z D/U$ (right) on

horizontal planes a at the level of a) 0.1D; b) 0.5D; c) 0.9D from the channel bed in case-S90 46

Figure 4-15 Two dimensional streamline patterns (left), mean streamwise velocity contours, u_s/U (middle) and mean out-of plane vorticity contours, $\omega_z D/U$ (right) on horizontal planes at the level of a) 0.1D; b) 0.5D; c) 0.9D from the channel bed in case-S135 47

Figure 4-16 Distribution of turbulent kinetic energy at the level of a) 0.1D; b) 0.5D; c) 0.9D from the channel bed for the mean flow in the case-S45(left), S90(middle) and S135(right) 48

Figure 4-17 Distribution of the pressure RMS fluctuations, $p'p'/\rho U2$ a) on the channel bed, b) on the outer bank and c) on the inner bank in case-S45 50

Figure 4-18 Distribution of the pressure RMS fluctuations, $p'p'/\rho U2$ a) on the channel bed, b) on the outer bank and c) on the inner bank in case-S90 51

Figure 4-19 Distribution of the pressure RMS fluctuations, $p'p'/\rho U2$ a) on the channel bed, b) on the outer bank and c) on the inner bank in case-S135 52

Figure 4-20 Non-dimensional shear stress distributions, $\tau_w/\rho V^2$, a) on the channel bed, b) on the outer bank, c) on the inner bank in case-S45 54

Figure 4-21 Non-dimensional shear stress distributions, $\tau_w/\rho V^2$, a) on the channel bed, b) on the outer bank, c) on the inner bank in case-S90 55

Figure 4-22 Non-dimensional shear stress distributions, $\tau_w/\rho V^2$, a) on the channel bed, b) on the outer bank, c) on the inner bank in case-S135 56

LIST OF SYMBOLS

B	mean channel width
C_{b1}, C_{b2}, C_{v1}, C_{w1}, C_{w2}, C_{w3}	Spalart Almaras model constants
C_{DES}	model constants
d	modified turbulence length scale
D	flow depth
d_{DES}	DES length scale
d_{min}	distance from a grid to the nearest wall
f_{v1}, f_{v2}, f_w	Spalart Almaras model constants
g^{ij}	contravariant metric tensor
h	Spalart Almaras model parameter
J	Jacobian of the geometric transformation
ks	equivalent roughness height
r	Spalart Almaras model parameter
R	mean radius of the curvature
Re	Reynolds Number
S	strain rate

$\check{S}$	Spalart Almaras model parameter
t	time
U	average flow velocity
u^j	contravariant velocity component in j direction
u_j	cartesian mean velocity component in j direction
x_i	cartesian coordinates
κ	Von-Karman constant
η	spanwise coordinate axis
τ_w	wall shear stress
ν	kinematic viscosity
$\breve{\upsilon}$	modified eddy viscosity
ν_t	turbulent eddy viscosity
ξ^i_{xj}	metrics of the geometric transformation
ξ^j	curvilinear coordinates in j direction
σ	Spalart Almaras model constant
χ	Spalart Almaras model parameter
ω_z	out-of-plane vorticity
Δ	local grid size
$\Delta_x, \Delta_y, \Delta_z$	grid spacings

LIST OF ABBREVIATIONS

DES	Detached Eddy Simulation
HV	Horseshoe vortex
LES	Large Eddy Simulation
RANS	Reynolds Averaged-Navier Stokes
RMS	Root-mean-square
SA	Spalart-Allmaras
TKE	Turbulence kinetic energy

CHAPTER 1

INTRODUCTION

1.1 Background

In natural rivers, the flow is turbulent and three dimensional and it never continues to be a straight line even in a straight river reach due to obstructions that affect the velocity field of the flow. The flow with a high velocity has more energy and it causes more erosion while the flow with a low velocity has less energy and so less erosion. Therefore, at the outer banks of the river, water cause erosion and at the inner banks, because of the less energy river deposits sediments. As a result of this situation, meanders form.

Due to the curvature of the meandering channel, centrifugal forces act on the flow and this causes the formation of the secondary flows. These secondary flows lead to the formation of the coherent structures that affect the erosion and deposition processes which are developing continuously (Constantinescu, Koken, & Zeng, 2011). Figure 1-1 shows the formation of the meanders and erosion and deposition processes.

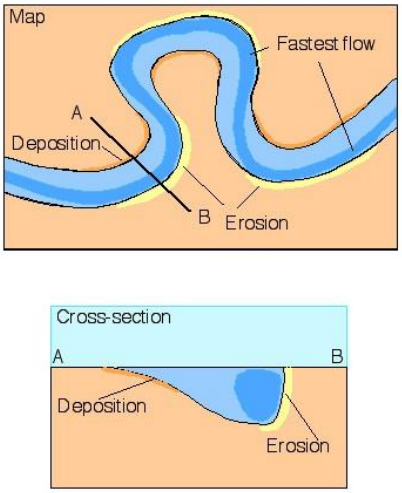

Figure 1-1 The formation of the meanders ("GCSE Rivers Revision - The Middle Course," n.d.)

Moreover, in a sharply curved channel (in which the ratio between the mean radius of the curvature (R) and the mean channel width (B) is smaller than 2) (Constantinescu et al., 2011) pool formation and bar formation are created because the high value of streamwise velocity alters towards the outer side and creates a pool while sediment deposition causes a bar formation at the inner bank (Blanckaert, 2010). The main cell of cross-stream circulation (i.e. flow particles form a helicoidal path) occurs only at outer and deeper part of the channel (Constantinescu et al., 2011).

In order to prevent scouring that is formed at the outer bank of the meandering channel, spur dikes are constructed. Spur dikes are river training structures that can be built at the bank of a river and can be elongated towards the main channel. They are mainly used for both in straight river reaches and in meandering rivers with the purpose of erosion protection and navigation improvement. Spur dikes are preferred among the other methods for erosion protection because they are the most economical structures (Azinfar, 2010). Figure 1-2 shows one spur dike example in Hiji River.

Figure 1-2 Typical spur dike in Hiji River in Japan ("Shallow Flow Visualization around a Single Groyne," 2007)

However the inclusion of the spur dike further complicates the flow field within a meandering reach which was already complex due to the curvature. When the flow approaches the spur dike, the incoming boundary layer separates due to the adverse pressure gradients. As a consequence of this, Horseshoe vortex (HV) system is created close to the channel bottom around the spur dike. Horseshoe vortices form at the upstream part of the obstruction and bends through the flow while it passes the obstacle. The HV system amplifies the turbulence kinetic energy and pressure root-mean-square fluctuations and bed shear stress along its mean path (Koken & Constantinescu, 2008a). These are the evidences of how HV system has an important role in the evolving of the scouring process.

There are many experimental and numerical studies which are related with the meandering channels or spur dikes in a straight channel reach which will be mentioned at Chapter 1.2. However there is no such study in the literature which investigates the coherent structures within a meandering channel with a spur dike numerically. With experimental studies, one can get only point or planar measurements within a limited area, which would not be adequate to identify the coherent structures along their whole length. On the other hand with a numerical

simulation once can obtain the solution throughout the whole flow domain. Thus, it is obvious that this kind of study cannot be an experimental one but rather should be a numerical study. Yet one should be careful in selecting the appropriate turbulence model. There are many turbulence models used in river engineering; such as Reynolds averaged Navier-Stokes (RANS) model, Large-eddy simulation (LES) model or Detached-eddy simulation (DES) model.

RANS turbulence model is the most popular numerical approach which is used in predicting complex engineering flows. RANS model is based on the time averaged mean flow. When the flow is massively separated and there are unsteady vortical structures, RANS model is not sufficient to predict the important aspects of the flow (Breuer, Jovičić, & Mazaev, 2003; Koken & Constantinescu, 2009)

On the contrary, eddy-resolving methods (LES or DES) are more successful when the flow is massively separated and there are unsteady vortical structures. Unlike RANS models a spatial filtering is applied to the Navier Stokes equations. In LES, all hydraulically important scales are resolved dynamically and only the smaller scales (subgrid) are modeled. However at a given Reynolds number, the computational grid must be fine enough and the time steps must be decreased to small enough for obtaining a good accuracy. In a LES model, especially when the use of wall function is avoided the demand for the computational resources highly increases as Reynolds number increases. Thus it is difficult to use LES model for flow problems which have high Reynolds numbers (Koken & Constantinescu, 2008a).

DES model is a hybrid method of RANS and LES models. The DES idea first explored with its formulation which is based on the Spalart-Allmaras (SA) turbulence model in 1997 (Strelets, 2001). It acts like RANS model near the solid surfaces and it acts like LES model away from the solid boundaries which considerably decreases the computational cost. It is shown that DES can accurately predict the presence of coherent structures within a turbulent flow (Koken &

Constantinescu, 2014). Moreover the bed shear stress and pressure RMS fluctuations on the bed which are very important in scour processes compared to experimental methods with DES. This is the main reason why DES is used in this study.

1.2 Literature Review

1.2.1 Studies related with Curved Channels

Blanckaert & Graf, 2001 investigated the flow in an advanced base topography in a curve. They performed experiments in a wide laboratory flume. The flume has vertical sidewalls which are made of plexiglass. The measurement section was at the 60° bending point in the outer bank of the channel. They presented the results of the mean velocities, turbulent stresses and turbulent kinetic energy distributions. They found that the cross-sectional movement involves two circulation cells; center-zone cell and outer-bank cell and they are observed in the corner of the water surface at the outer bank. Also the flow velocity in the outer half section was greater than the flow velocity in the straight flow and the core of the maximum velocities are located very close to the water surface, close to the distance between both circulation cells. Moreover they investigated that the turbulence structure in a curve differs from that of a straight stream, most particularly toward the outer bank, there is a reduction of the turbulence activity. They concluded that the stability of the flow parameter and the bending morphology are influenced by the outer bank cell and reduced turbulence activity because they may protect the outer bank and adjacent base.

Blanckaert & De Vriend (2004) made another study with the same experiment setup to investigate the secondary flow in a sharp bend channels. They observed a weaker and smaller reverse circulation cell in addition to the classical spiral movement near the outer bank and this can play an important role in bank erosion. They provided detailed experimental data on both centre-zone cell and outer bank cell in open channel bend with that study and they investigated the fundamental dynamics by simultaneous analysis which deals with the vorticity equation and kinetic energy

transfer between the mean and turbulence flow. Results showed that turbulence has a minor role in the formation of the centre zone cell. With the relationship between the downstream velocity profile and centre zone cell, accurate estimation of velocities in the middle zone is yielded by strongly simplified vorticity balance. They found that the centrifugal force supports the outer bank cell due to the non-uniform velocity profiles and the terms of the anisotropy of cross-current turbulent caused by border proximity substantially enhance the outer bank cell. Moreover the formation of the outer bank cell has been shown to be dependent not only on the flow instability but also on the turbulent kinetic energy input as in the curved laminar flow case.

Dehghani A.A., Ghodsian M., Suzuki K. (2008) investigated experimentally how the position of lateral intake affects the maximum local scour depth in a 180° curved channel. Local scour formed near the lateral intake because the streamlines are curved and tended towards to lateral intake which caused formation of vortices. In their study, they situated the lateral intake on 90, 115 and 150 degrees. The results showed that near the lateral intake, two scour holes are formed; one of them is at the upstream edge and the other one is at the downstream edge of the intake. Furthermore, they found that maximum scour hole depth occurred on 90° intake and longest scour hole length formed on 150° intake.

Blanckaert (2009) investigated the effect of the saturation of the energy losses, turbulence and secondary flow due to the curvature in open channels with sharp bends. The experimental flume has rectangular cross-section along a 193° bend with constant curvature radius. Experiments were repeated for three different curvature ratios, i.e. the ratio between the centerline curvature radius and flow depth. The study showed that the secondary flow no longer increases when the curvature ratio exceeds a certain threshold value. This situation is called saturation. They also observed the similar phenomenon for the turbulence and energy losses. Secondary flow was discussed to be a dominant factor for increasing energy losses which is due to increased turbulence production caused by curvature.

The effects of the three-dimensional flow field, the secondary flows and the shear stresses on a strongly curved 193° bend were studied by Constantinescu et al. (2011). The channel bed was fixed which corresponded to a deformed bed conditions at the latest stages of the scour process. They used the DES model at a Reynolds number of 68400. They compared the results of the DES model with experimental results and the results of a RANS model. They found that DES predicted that in the deeper part of the bend the main cell of cross stream circulation developed and at the inner bank several streamwise oriented vortex (SOV) cells are formed. Compared to the experiment, DES predicted the streamwise velocity, streamwise vorticity, the velocity distribution and the vortices more accurately than the RANS model. Furthermore, the mean flow bed shear stress distribution is predicted more accurate by the DES model. Then they used the DES model to explain the effects of the streamwise oriented vortex cells and separated shear layers on the boundary shear stress.

The flow processes near the outer bank in curved channels on the basis of bank roughness was investigated by Blanckaert, Duarte, Chen, & Schleiss (2012) in a laboratory flume. They examined for all the roughness configurations on the outer bank the reverse secondary flow occurs. They found that the cell expands the boundary layer on the outer bank which causes the flow forcing reduction while at the same time advancing of high momentum fluid toward increases the flow forcing on the bank. Furthermore increasing in the roughness of the outer bank resulted in significant expansion and strengthening of the outer bank cell. Effective width of the channel where most of discharge is transmitted was reduced by the expansion of the boundary layer on the outer bank and that leads to higher sediment transport capacity in the middle section of the channel was investigated. They also found that the outer bank cell reaches the maximum vulnerability in the most strength zone against the bed scour and erosion that supports the morphological appropriateness.

Koken, Constantinescu, & Blanckaert (2013) investigated the flow physics in open channel which has a sharp bend and a flat bed. They used eddy-resolving numerical

methods and completed the simulation with experiments. They focused on the effects on the coherent structures and contributions of these structures on shear stresses and flow capacity. They also focused on the results that are changing with the increasing Reynolds number with laboratory models and field conditions. The results showed that laboratory models and field conditions indicate similar flow processes although some scale effects exist with different Reynolds number. Moreover they discussed the implementation of some improved methods for the purpose of estimating average sediment uptake rates in sharp bends.

1.2.2 Studies related with Spur-dikes

Azinfar & Kells (2007) studied the backwater effect occurred due to a spur dike in a laboratory flume. They used a single, vertical-walled spur dike. Momentum principle was used for the analysis of the flow regime. For momentum principle, drag coefficient represented the resistance which occurred due to the spur dike. At the end, they found that in an open channel flow, backwater effect of the spur dike is a function of the contraction which occurred with the inclusion of the spur dike, the submergence ratio, the aspect ratio of the spur dike and the Froude number of the flow. The results show that while the submergence ratio has the greatest contribution on the backwater effect, the Froude number has the smallest influence.

Koken & Constantinescu (2008a) investigated the flow physics and the effects of the coherent structures around a vertical spur dike at the start of the scour in a straight channel. They used the LES model at a Reynolds number of 18000. They also made visualization experiments for understanding the role of the interactions between the coherent structures. They found that the main vortex path of the HV system around the spur dike change in time and positions considerably. However one path was observed at all times but its intensity and coherence was variable. Figure 1-3 shows a sketch model around the spur dike. They also found that main path of the vortex oscillates aperiodically between two states; one of them is zero-mode flow (in which the vortex is closer to spur dike) and the other one is back-flow mode (in which the

vortex is away from the spur dike). They also observed that because of the interactions between the legs of the horseshoe vortices, the necklace vortex loses its coherence considerably.

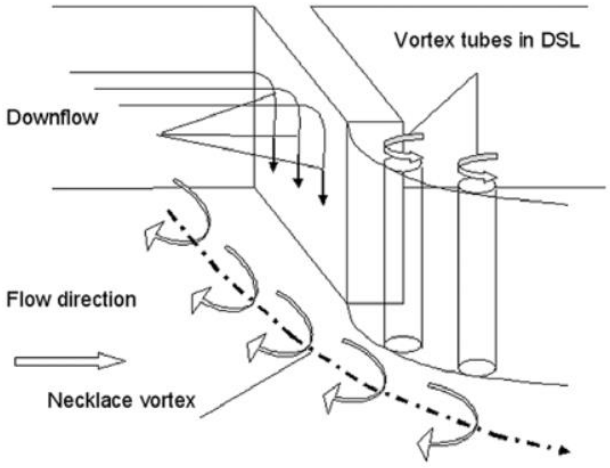

Figure 1-3 Sketch of the main coherent structures and physical phenomena present around an isolated spur dike (Koken & Constantinescu, 2008a)

Koken & Constantinescu (2008b) also conducted a study to investigate the flow physics and coherent structures around a vertical spur dike at the later stages of the scouring process in a channel. The channel is straight and has equilibrium scour bathymetry. The bathymetry was obtained with an experiment and LES model is used at a Reynolds number of 18000. They found that the main necklace vortex was parallel to the spur dike and then wrapped around its tip. Like flat bed case, the intensity and the coherence of the HV system changed in time considerably. They investigated that the chaotic oscillations were also presented inside the HV region when the bed is deformed. When the horseshoe vortex system has the largest coherence, it is seen that the distributions of pressure root-mean-square fluctuations and turbulence kinetic energy have two peaks. Moreover the investigation showed that the vorticity patches move against the slope of the scour hole mainly in the main channel and produce the sediment entrainment. The study showed that the 3D eddy-

resolving simulations can be used for the erosion mechanisms for better understanding.

Shafaie, Ardeshir, Sadat-Helbar, & Saneie (2008) investigated how the spur dike's length and orientation affect the scouring at the first spur dike within a series of spur dikes. They used four spur dikes with same spacing which are equal to two times the length of the first spur dike. Figure 1-4 shows the definition of the experimental flume of their study. They repeated the experiments for three different minor spur dike lengths with three different flow depths where minor spur dike was installed at three different location. It was shown that to preserve the spur dike from scouring, the ratio between the lengths of minor spur dike to first spur dike should be taken into consideration.

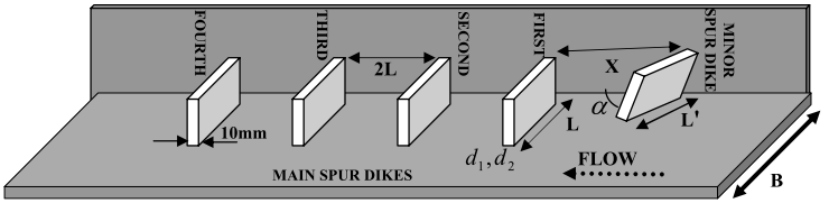

Figure 1-4 Definition sketch (Shafaie et al., 2008)

Koken & Constantinescu (2011) made another numerical study related with spur-dike structure. They used DES simulation to investigate the flow and turbulence structure in a straight channel with a vertical-wall spur dike. In DES simulation and in experiment Reynolds number of 240000 was used. They used DES for the typical applications in small rivers and LES can be conducted in outside of range. From a loose bed experiment the bathymetry was obtained. They discussed the main mechanisms that affect the growing of scour hole around the spur dike during the scour process in later stages and how the initial and later stages of the scour process are altered due to those mechanisms. They also investigated the scale effects by comparing the results of simulations with Reynolds number of 240000 and much lower Reynolds number of 18000. Results showed that the main necklace vortex of

the horseshoe vortex system is affected by large scale aperiodic oscillations although the structure of the HV system alters with respect to the flat bed case. Study showed that LES and DES predicted much closer results inside the seperated shear layer and wake regions and also experiments revealed that the flow at higher Reynolds numbers is affected by large scale oscillations of the main vortex more strongly.

Koken (2011) studied numerically the effect of spur dike angle with respect to the flow direction on the coherent structures forming around it. DES model is used at a Reynolds number of 45000. He investigated three different flow angles of spur dikes which are 60, 90 and 120 degrees. He found that the HV system has changed considerably with different flow angles and the size of the main horseshoe vortex and the possible scour area is largest in 90° case compared to 60° and 120° cases.

Koken & Constantinescu (2014) investigated the effects of an isolated spur dike with sloped sidewalls at the start of the scour process experimentally. The spur dike was protected against the scouring with a riprap apron. The effects of large-scale turbulence on the sediment entrainment and transport are also discussed. They used the previous results of the eddy-resolving numerical simulations for their research. With the information gathered, some reasons for the bed scour patterns at the end of the scour process for the cases with and without a riprap apron were investigated. The bluntness of the upstream side of the abutments is characterized as lower degree compared with vertical-wall abutment of similar length. They investigated that this difference has an important effect on the coherent structures around the spur dike. Their study showed that eddy-resolving numerical simulations can be used for understanding the vortical structure and determining where riprap can be placed to avoid the large scale of scouring.

Koken & Gogus (2014) investigated the effects of the spur dike length on turbulent flow structures in a horizontal channel both numerically and experimentally. They studied for examining how horseshoe vortex system, bed shear stress and the pressure standard deviation at the bed are changing with different spur dike’s length.

With this purpose, they used three different lengths in their study. They used DES model with a channel Reynolds number of 45000. At the end of the study, they investigated that at all lengths, horseshoe vortices were formed around the spur dike however the main HV was less coherent in the shortest spur dike case. With the increasing length of the spur dike, the magnitudes of the large bed shear stress and pressure RMS fluctuations increased around the tip of the spur dike.

1.3 Scope of the Study

The objective of this study is to investigate the coherent structures and their influences on the flow dynamics by using the eddy resolving method Detached Eddy Simulation. For this purpose different spur dike configurations are simulated in a 180 degrees channel bend that has a flat bed. At the end of this study the changes in the flow field and coherent structures are understood.

1.4 Thesis Organization

The layout of this study is as follows: A brief introduction and a literature review are presented in Chapter 1. In Chapter 2, necessary formulations of Spalart-Allmaras based DES model used in the calculations are given. Moreover main parameters, computational domain, used mesh and boundary conditions in the models are explained. In Chapter 3, the results of the simulation of case without spur dike are discussed. Also grid dependence check is done in this chapter. In Chapter 4 the results of three cases with spur dike are discussed. Finally, in Chapter 5 conclusions are drawn.

CHAPTER 2

NUMERICAL MODEL

2.1 Spalart-Allmaras One Equation Model

In the Spalart-Allmaras (SA) linear eddy viscosity model, together with the Navier Stokes equations, an additional transport equation is solved for the modified eddy viscosity, $\tilde{\nu}$ to form the turbulent eddy viscosity, ν_t.

The transport equation for $\tilde{\nu}$ is;

$$\frac{\partial \tilde{\nu}}{\partial t} + u^j \frac{\partial \tilde{\nu}}{\partial \xi^j} = C_{b1}\tilde{S}\tilde{\nu} + \frac{1}{\sigma}\left[J\frac{\partial}{\partial \xi^j}\left(\frac{g^{ij}}{J}(\nu + \tilde{\nu})\frac{\partial \tilde{\nu}}{\partial \xi^j}\right) + C_{b2}\left(\frac{\partial \tilde{\nu}}{\partial \xi^m}\xi^m_{xj}\right)\left(\frac{\partial \tilde{\nu}}{\partial \xi^1}\xi^1_{xj}\right)\right] - C_{w1}f_w\left[\frac{\tilde{\nu}}{d}\right]^2 \quad (1)$$

where t is the time and u^j contravariant velocity components and can be defined as;

$$u^j = u_j \xi^j_{x_i} \quad (2)$$

J is the Jacobian of the geometric transformation;

$$J = \frac{\partial(\xi^1, \xi^2, \xi^3)}{\partial(x_1, x_2, x_3)} \quad (2)$$

g is the contravariant metric tensor;

$$g^{ij} = \xi^i_{xk}\xi^j_{xk} \quad (3)$$

S is the strain rate and;

$$\tilde{S} = S + \left(\frac{\tilde{\nu}}{\kappa^2 d^2}\right) f_{v2} \quad (4)$$

$$f_{v2} = 1 - \tilde{\nu}\left(\frac{1}{Re} + \tilde{\nu} f_{v1}\right) \quad (5)$$

$$f_{v1} = \frac{\chi^3}{\chi^3 + {C_{v1}}^3} \quad (6)$$

$$\chi = \frac{\tilde{\nu}}{\nu} + 0.5\frac{k_s}{d} \quad (7)$$

the function f_w is;

$$f_w = h\left[\frac{1+{C_{w3}}^6}{h^6+{C_{w3}}^6}\right]^{1/6} \quad (8)$$

$$h = r + C_{w2}(r^6 - r) \quad (9)$$

$$r = \frac{\tilde{\nu}}{\tilde{S}\kappa^2 d^2} \quad (10)$$

d is the modified turbulence length scale and can be defined as;

$$d = d_{min} + 0.03k_s \quad (11)$$

where, d_{min} is the distance from a grid point to the nearest wall and k_s is the equivalent roughness height, u_i is the cartesian mean velocity components, x_i is the cartesian coordinates and ξ^i is the curvilinear coordinates.

The constants in the above equations are as follows: C_{b1} = 0.135, C_{b2} = 0.622, σ = 0.67, κ = 0.41, C_{v1} = 7.1, C_{w2} = 0.3, C_{w3} = 2.0 and $C_{w1} = C_{b1}/\kappa^2 + (1+C_{b2})/\sigma \approx 3.224$

Finally the eddy viscosity ν_t is obtained from;

$$\nu_t = \tilde{\nu} f_{v1} \quad (12)$$

2.2 Spalart-Allmaras based DES model

In the SA based DES model, d is replaced with a new length scale d_{DES}. d_{DES} is defined as;

$$d_{DES} = \min(d, C_{DES}\Delta) \quad (13)$$

where C_{DES} is the model constant and equal to 0.65; Δ is the local grid size and can be defined as $\Delta=\max(\Delta_x, \Delta_y, \Delta_z)$. ($\Delta_x$, Δ_y and Δ_z are the grid spacings.)

Near the solid surfaces Δ is larger than d and so RANS model is used to predict the flow because the standard SA model does not change. Away from the solid surfaces, since $\Delta< d$, the equation shows that $\tilde{\nu} \sim S\Delta^2$ (S is the total absolute vorticity) and this shows that Smagorinsky eddy viscosity is yielded and LES model is used. (Constantinescu & Squires, 2004; Koken & Gogus, 2014)

2.3 Main Parameters, Computational Domain and Mesh

Results of five cases are discussed in this study. In all cases, same channel dimensions are used for the cases that contained the spur dike. Same spur dike dimensions are used except its length at different angles with the flow. The length of the spur dike is selected so that the contraction generated in the channel is nearly 0.25 of the width at all cases. Simulations are non-dimensionalized by the flow depth, D and the average flow velocity, U, which are 0.15 m and 0.83 m/s, respectively. Figure 2-1 shows all the dimensions used in the models. The flume has a straight incoming reach of 33D length which is bending to 180 degrees with a channel curvature of R which is measured as 10D from the channel centerline. Then bending is followed with straight outcoming of 45D length. Channel width, B is 8D. In three simulations, spur dike is located on the outer bank of the channel at 30 degrees from the starting of the bend. The length and the width of the spur dike in all simulations are 2D and 0.33D, respectively. Spur dike is tangent to the channel with an angle of 45, 90 and 135 degrees.

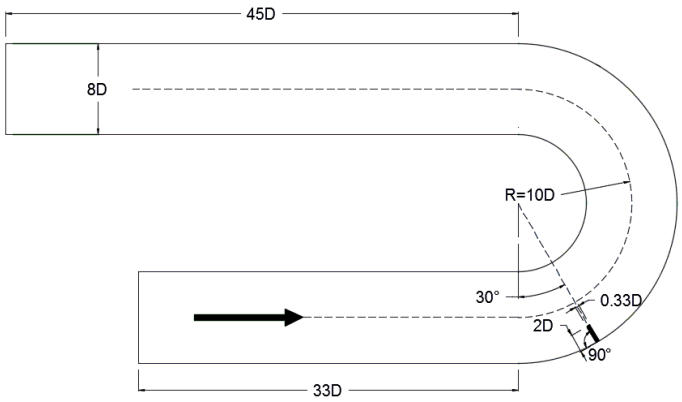

Figure 2-1 General sketch of the model

The Reynolds number and the Froude number of the channel which are calculated using the flow depth at the inlet and the average velocity are around 125000 and 0.68, respectively.

Computational mesh is created with a structural grid generation software. Some parameters are taken into consideration while creating the mesh. One thing is that in order to resolve viscous sublayer, y^+ is taken as one and the first grid point near the wall is situated according to that. Meshes are created with nearly right angles, especially close to the walls and smooth mesh transition is utilized between the coarse and fine mesh regions. In the simulations with spur dikes and one simulation without the spur dike meshes are structured with 768x168x33 nodes in the streamwise, spanwise and vertical directions, respectively (about 4.3 million grid points are used). In one simulation without the spur dike, a coarser mesh size with 720x132x33 node is used. The coarser mesh which has about 3 million grid points is used in the grid dependence study which will be discussed in Chapter 3.1.

Since the DES code was not able to predict the free surface deformations FLOW 3D software is used to obtain the free surface patterns for different cases. 3D flow simulations are conducted for all the cases in FLOW 3D until steady-state conditions are reached. After a grid dependence check 0.015 m uniform grid spacing is used in all of these simulations. Discharge is specified at the inlet where no slip boundary

condition is used along all the solid walls. Two equation (k-ε) model is used. Inflow and outflow boundary conditions are selected as pressure; however for inflow condition fluid elevation is given as 0.17 m and for outflow condition fluid elevation is given as 0.15 m. In order to define flow direction, mass flux is placed at outflow. Top side of the boundary condition is selected as pressure with a fluid fraction as zero to get the open channel flow. In order to get continuity between two components symmetry condition is selected and the other boundary conditions are selected as wall condition. Figure 2-2 shows these boundary conditions. Obtained free surface topographies are extended to not conflict with the created mesh and non-dimensionalized with the flow depth, D. After that the topography is exported as ASCII data file and then it is imported into the mesh that will be used in the DES code. In Figure 2-3 one Flow 3D solution can be seen.

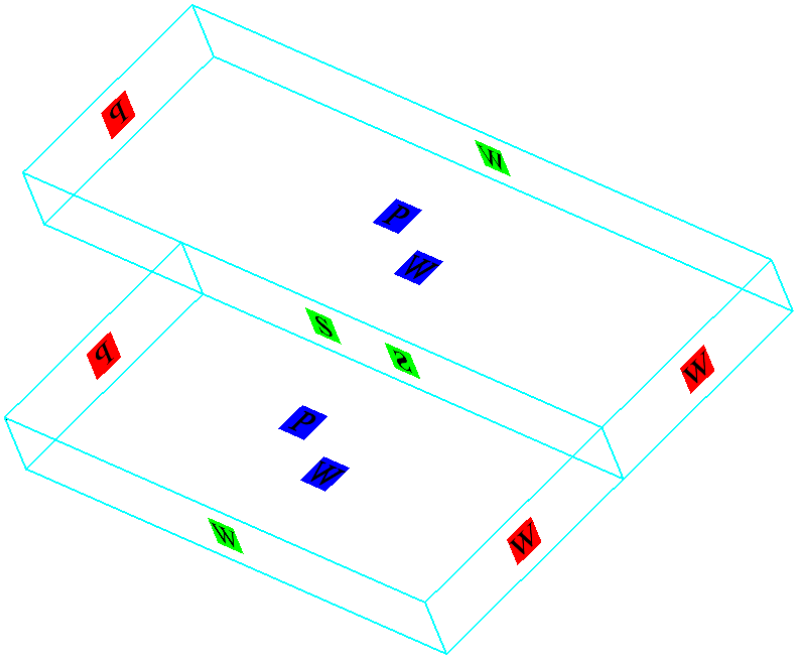

Figure 2-2 Boundary conditions of Flow 3D simulation (P: pressure condition, W: wall condition, S: symmetry condition)

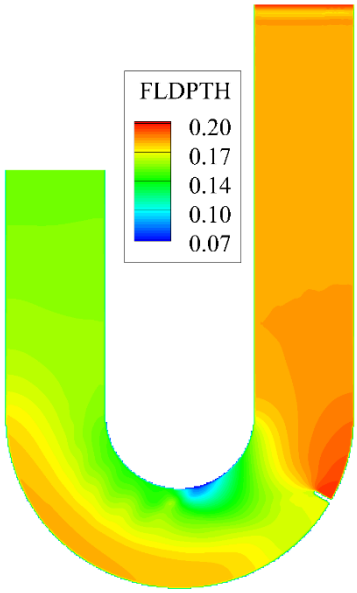

Figure 2-3 One Flow 3D solution

At the start of the simulations, the RANS model is run until a steady-state condition is reached. The RANS solution is then stored and used as an initial condition for the DES simulations. In the DES simulation, iterations are continued until a statistically steady-state condition is reached. The time step used in the simulations is 0.02D/U. Current code is parallelized with MPI (Message Passing Interface). The simulations are run on 12 processors of a PC cluster. The processor of the cluster is 2x Intel Xeon i5-2690. After statistically steady-state condition is reached, data are collected to get statistics for approximately a duration of 50D/U.

2.4 Boundary Conditions

At the inflow section, a velocity profile containing turbulent fluctuations is fed in a time-accurate fashion. The profile is obtained from another LES simulation which is performed in a periodic channel with the same section and about the same Reynolds number.

At the outflow section, a convective boundary condition is used. This condition provides the flow to exit from the domain in a time accurate way and prevents formation of unphysical oscillations.

No slip boundary condition is used along all solid walls. Free surface topography obtained from Flow 3D simulation is used as a rigid lid in the DES simulations.

CHAPTER 3

ANALYSIS OF THE MEAN AND INSTANTANEOUS FLOW STRUCTURES IN THE CURVED CHANNEL WITHOUT SPUR DIKE

3.1 Grid Dependence Study

For the purpose of controlling the grid dependence two models are created one with a finer mesh (4.3 million grid points) and one with a coarser mesh size (3 million grid points. In this part, some flow phenomenon is compared for these two models which have the same initial and boundary conditions. When the results are compared, it is decided that both mesh sizes are sufficient to capture the flow physics. In order to control the sufficiency some parameters are compared at the same section. In Figure 3-1, non-dimensionalized streamwise vorticity magnitudes and streamline patterns for the mean flow are compared at section D60 for both finer and coarser mesh simulations. In the figure, η is the spanwise coordinate axis. One can clearly observe that streamwise vorticity contours are similar in both simulation. On the whole channel section high amplification in streamwise vorticity is observed because of the secondary flow in the channel. Furthermore, in both cases around the outer bank close to the free surface a negative vorticity patch is seen. This is as a result of a streamwise oriented vortex close to the free surface. Streamline patterns at this location in both simulations confirm the presence of this vortex. Since the coarser and finer mesh sizes give similar results, it can be said that the solution is grid

independent. Finer mesh size captured the outer cell vortex better. Thus, the finer mesh size is selected and used throughout the rest of this study.

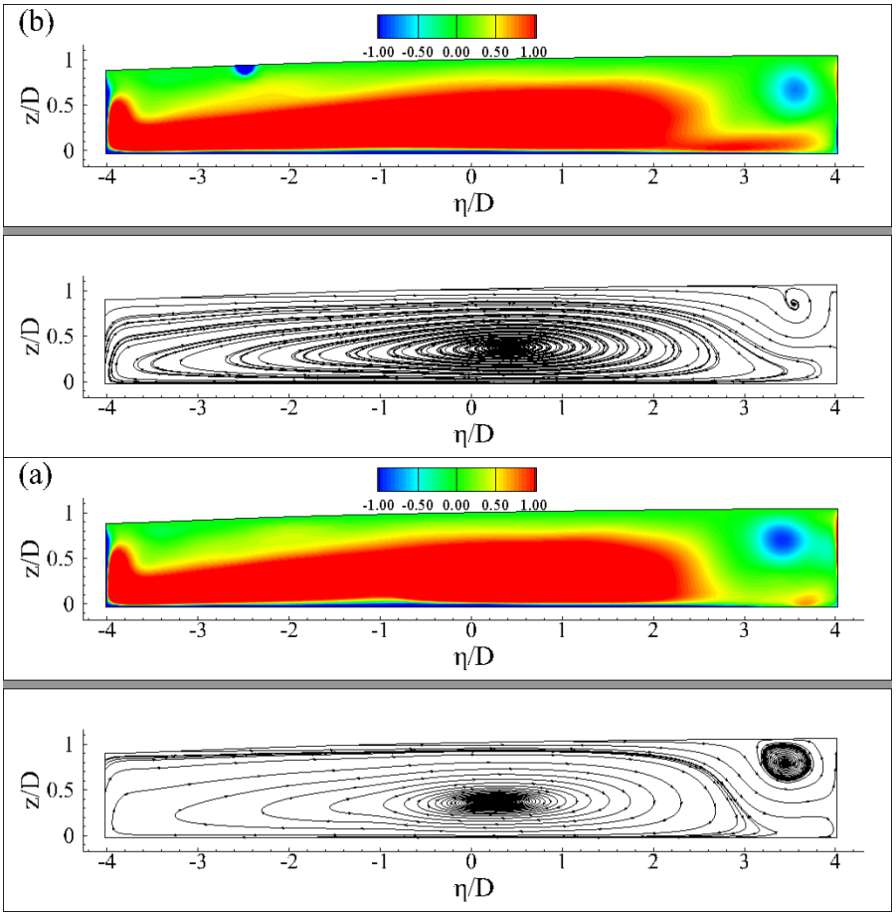

Figure 3-1 Non-dimensional mean streamwise vorticity distributions and corresponding streamline patterns at section D60 at a) finer mesh size case, b) coarser mesh size case

3.2 Description of the Main Vortical Structures in the Mean Flow

Several streamwise oriented vortices (SOVs) are formed within the channel bend because of the high curvature. The Q criterion is used to visualize the SOV cells for the mean flow (see Figure 3-2). The Q criterion is the quantity that visualize the vortical structures and it is the second invariant of the velocity gradient tensor

$\left(Q = -0.5\left(\frac{\partial u_i}{\partial x_j} \times \frac{\partial u_j}{\partial x_i}\right)\right)$ (Constantinescu et al., 2011). Figure 3-2 shows that three SOV cells are observed within the channel. One of them is close to the inner bank, VI, the other one is close to the outer bank, VO, and the last one is in the middle of the channel, VM. VI is initiated close to section D60 while VO is initiated just upstream of section D60. Both VI and VO extend along the bank they are initiated. One difference between VI and VO is that VO forms close to the free surface whereas VI occupies the whole flow depth (see Fig. 3-4e). Vortex VM is initiated around section D30 close to the outer bank and then follow the path in the streamwise direction towards the inner bank.

In the instantaneous flow the coherent structures visualized using the Q criterion is shown in Figure 3-3. There are big differences in coherent structures between the mean flow and instantaneous flow. In the instantaneous flow it can be seen that the flow structure is more chaotic with lots of small scale coherent structures populating the flow domain. It is interesting to note that although there are coherent structures associated with VI and VM there is not a trace of VO at this time instant.

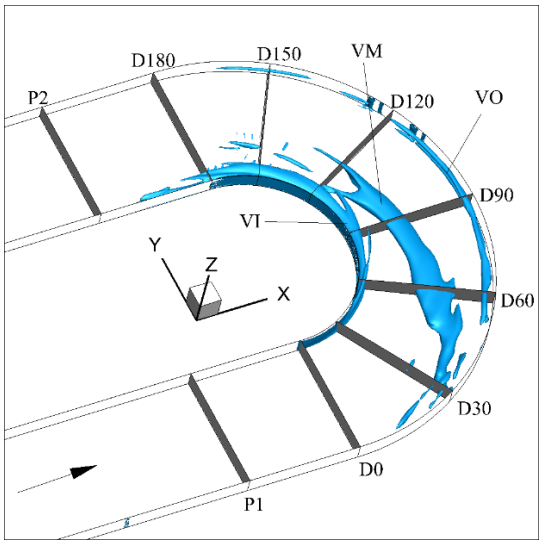

Figure 3-2 Three dimensional visualization of the vortical structure of the mean flow using the Q criterion

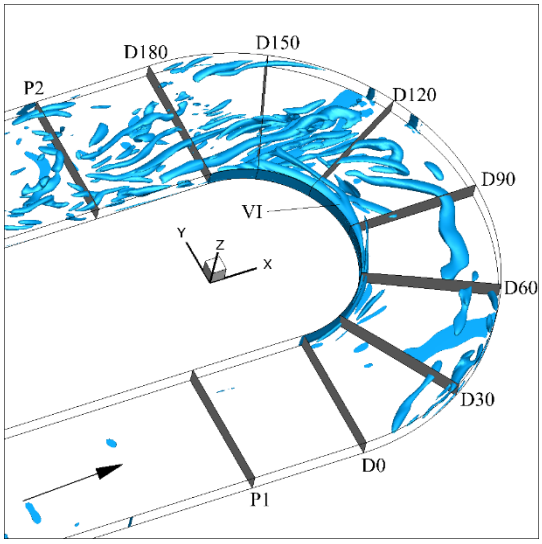

Figure 3-3 Three dimensional visualization of the vortical structure of the instantaneous flow using the Q criterion

Figure 3-4 shows the streamline patterns on several vertical sections. Streamline patterns clearly shows the SOV cells within the bend. Figure 3-5 shows the streamwise vorticity contours on the same vertical sections. Largest streamwise vorticity values are observed at section D90 where cross-stream circulation is strongest. Streamwise vorticity contours are also amplified along the mean positions of SOV's. As a result at sections D60 and D90 it is possible to distinguish vortices VI and VO. However the amplification due to the secondary flow in the channel prevents the identification of VM within the channel except at section D30. One can observe that VO loses its coherence at section D120. At this section it is not possible to distinguish VI and VM as they get very close to each other close to the inner bank.

Figure 3-6 shows the non-dimensional streamwise velocity contours at the same sections. It can be understood from the figure that the high core of streamwise velocity shifts towards to inner bank when the flow enters into the bend. At section D30 the highest streamwise velocity magnitude is observed. Also at the same section the separation zone is clearly seen due to the negative velocity magnitudes near the outer bank. Through the bend the highest streamwise velocities are observed close to

the inner bank. On the other hand large streamwise velocity magnitudes are observed along the outer bank once flow leaves the bend.

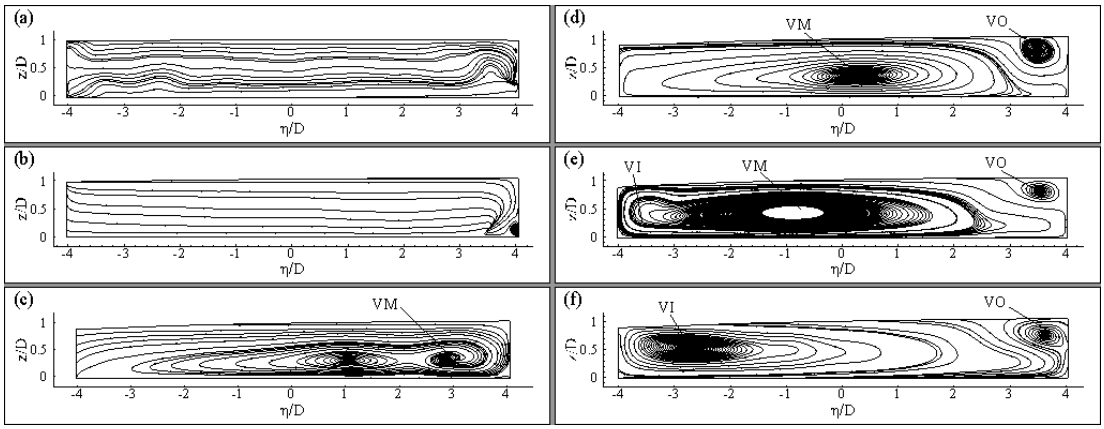

Figure 3-4 Mean streamline patterns at sections a)P1, b)D0, c)D30, d)D60, e)D90, and f)D120

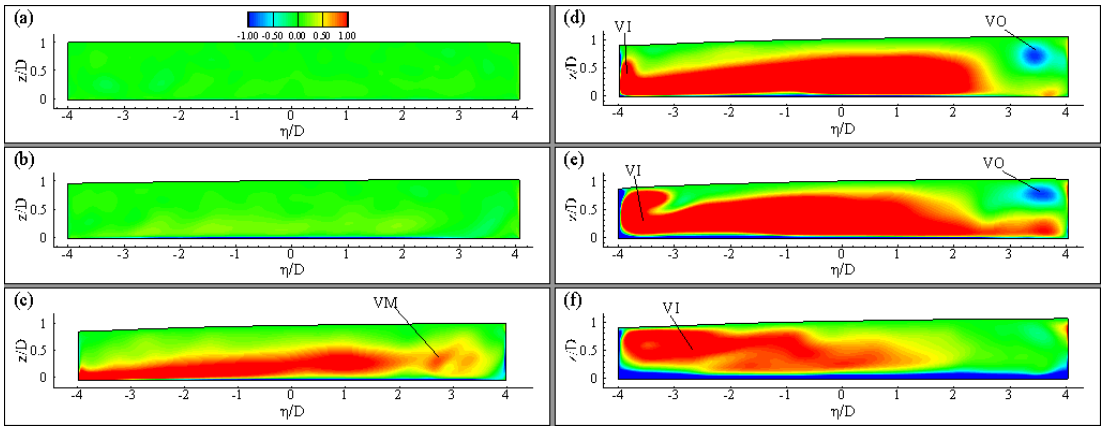

Figure 3-5 Mean streamwise vorticity distributions at sections a)P1, b)D0, c)D30, d)D60, e)D90, and f)D120

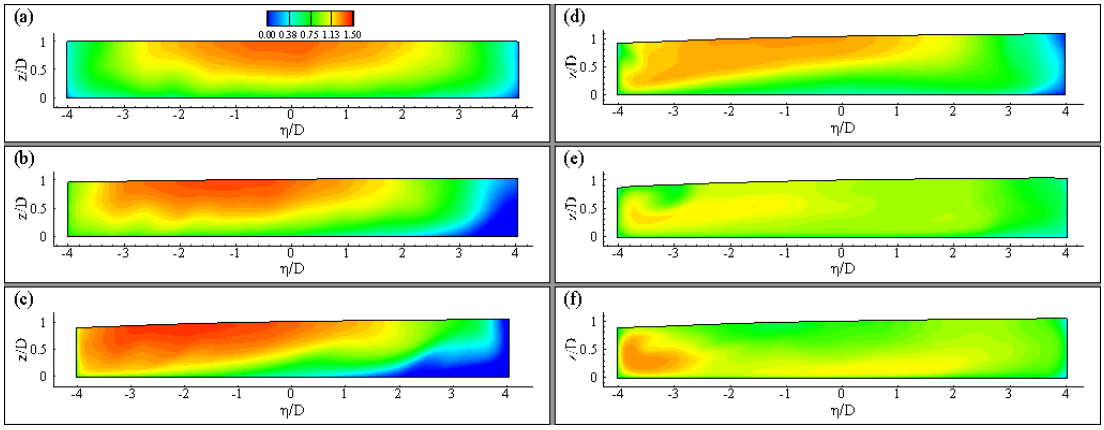

Figure 3-6 Mean streamwise velocity distributions at sections a)P1, b)D0, c)D30, d)D60, e)D90, and f)D120

3.3 Description of the Seperated Shear Layers and the Turbulence Kinetic Energy Distribution

In Figure 3-7 two dimensional streamline patterns, non-dimensional streamwise velocity and out-of-plane vorticity contours are shown on horizontal planes close to the channel bed, mid-depth and at the free surface of the channel. Large streamwise velocity magnitudes observed initially at the center of the channel initiates towards the inner bank once flow enters into the bend. On the other hand, at the exit of the bend large velocity magnitudes are observed close to the outer bank (see Figure 3-7 middle column). Moreover, negative velocity values are observed around section D0 at all flow depths. One can see an energetic shear layer between sections D60 and D120 close to the inner bank which is the strongest at the free surface and loses its coherence close to the channel bend (see Figure 3-7 right column). Formation of this shear layer is because the streamline patterns cannot follow the curvature of the inner bank and hence a slow moving fluid region near the inner bank. This shear layer is actually between the high speed flow which is in the mid-channel and slow moving fluid which is close the inner bank. Moreover some large vorticity magnitudes are seen close to the outer bank. It is seen that these are formed as a result of flow separation along the outer bank at the upstream of section D0.

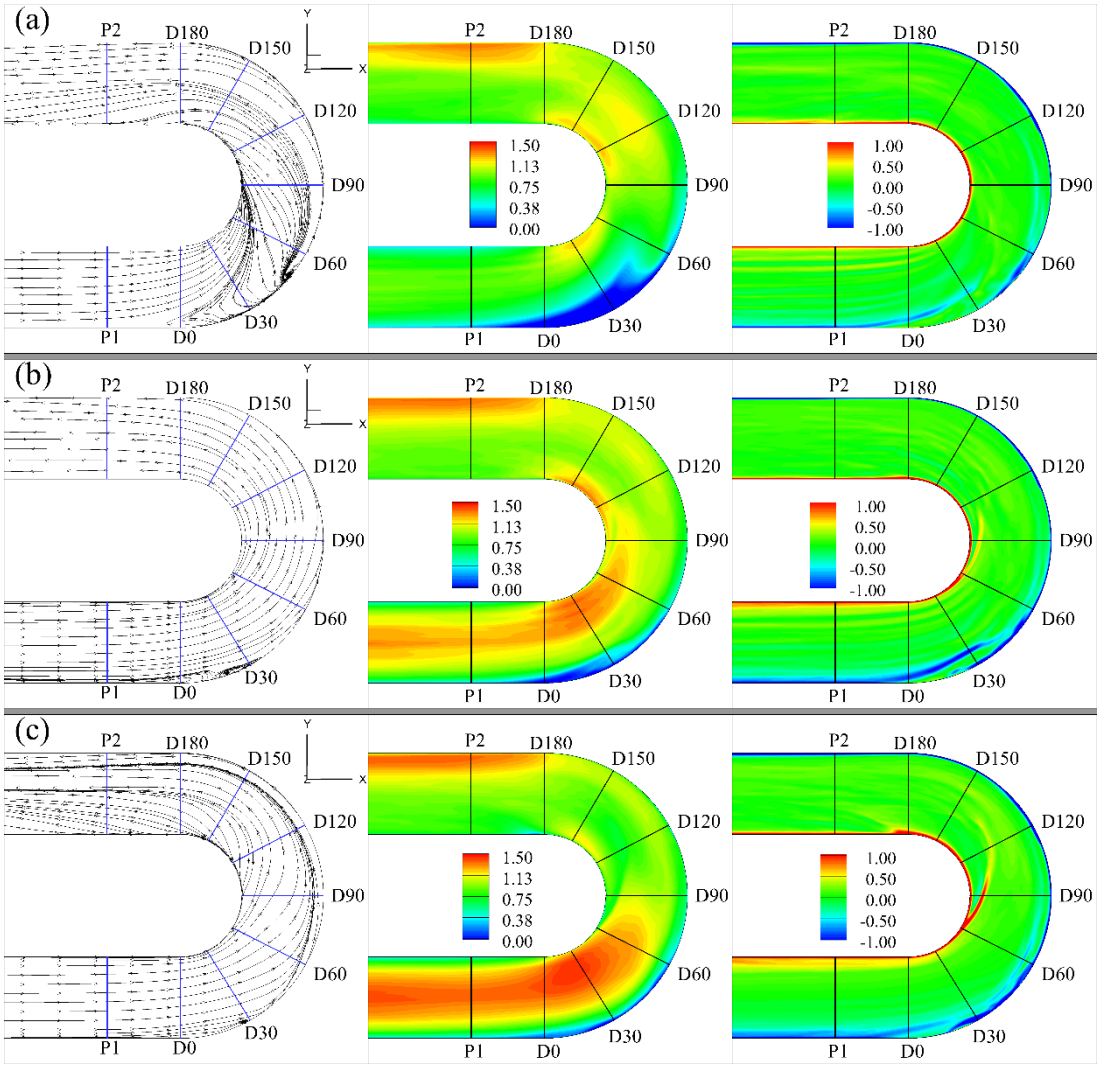

Figure 3-7 Two dimensional streamline patterns (left), mean streamwise velocity contours, u_s/U (middle) and mean out-of plane vorticity contours, $\omega_z D/U$ (right) on horizontal planes at the level of a) 0.1D; b) 0.5D; c) 0.9D from the channel bed

In Figure 3-8 out-of-plane vorticity contours on horizontal planes are shown for the instantaneous flow. Similar to Figure 3-7 in the instantaneous flow we can see the energetic shear layer forming close to the inner bank which was also observed in the mean flow together with lots of small scale vorticity patches especially between sections D90 and D180.

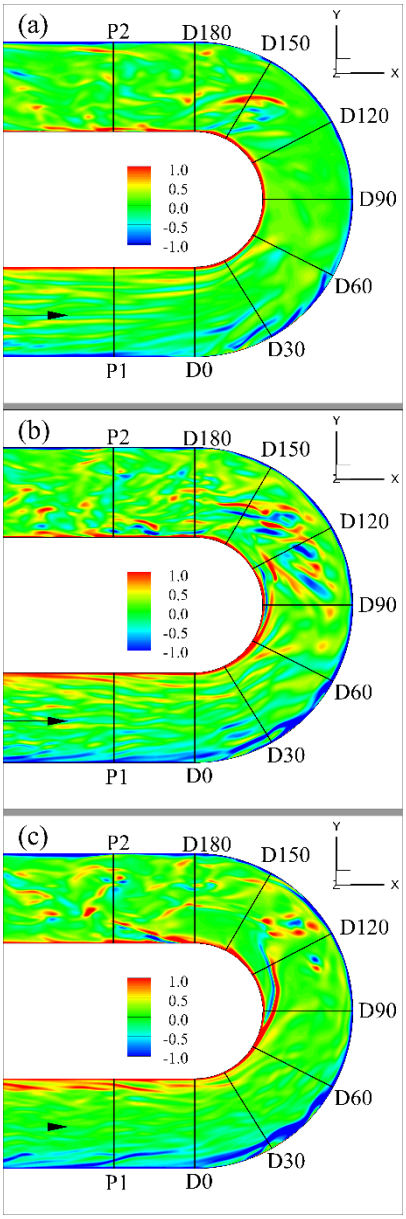

Figure 3-8 Mean out-of plane vorticity, $\omega_z D/U$ contours for instantaneous flow at the level of a) 0.1D; b) 0.5D; c) 0.9D from the channel bed

In Figure 3-9 non-dimensional turbulent kinetic energy distribution is shown on horizontal planes. High TKE values are seen between the sections D100 and D180 close to the inner bank at all depths. This is associated with the small scale energetic structures seen within this region in the instantaneous flow (see also Figures 3-3 and 3-8). Another region where high TKE values are observed is between sections D30

and D90; close to the outer bank. Amplified TKE values here is observed only close to the free surface and is not present close to the free surface and is not present close to the channel bed since this amplification is related to the presence of vortex VO. One last amplificant region in TKE values is observed close to the outer bank between D0 and D60 near the channel bed. This is as a result of the secondary flow and vortex VM.

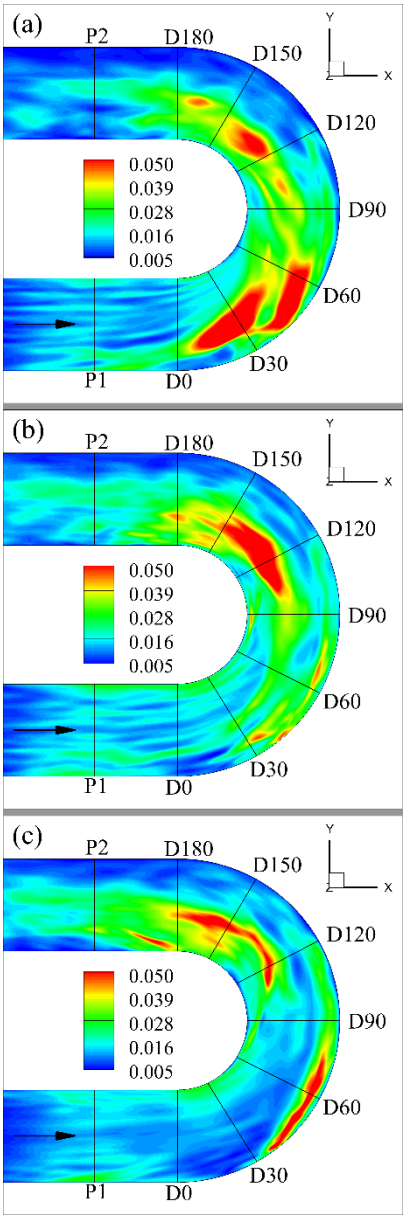

Figure 3-9 Distribution of turbulent kinetic energy for the mean at the level of a) 0.1D; b) 0.5D; c) 0.9D from the channel bed

3.4 Pressure RMS Fluctuations and the Shear Stress Distributions

Pressure root-mean-square fluctuations is an important parameter which contribute to the entrainment of sediment particles on the bed and thus to scour.

Figure 3-10a shows the pressure RMS distributions on the channel bed. Although the distribution is uniform at the channel entrance when the flow enters into the bend larger pressure RMS fluctuations are observed along the inner bank. The highest non-dimensional pressure RMS fluctuation value is 0.66, which is observed close to inner bank after section D30. The amplified regions shows correlation with the main path VI and VM (see Fig.3-2).

Pressure RMS fluctuations on the inner and outer banks are given in Figure 3-10b and 3-10c.

In order to see the banks in a straight plane a basic computer program is written. Three dimensional coordinate plane is transformed into two dimensional coordinate plane. In order to achieve this transformation ζ value is found by using this formula:

$$\zeta_{n+1} = \zeta_n + \sqrt{(x_{n+1} - x_n)^{2+}(y_{n+1} - y_n)^2} \quad (14)$$

where x_{n+1}, x_n, y_{n+1}, and y_n is the 3D coordinate points and ζ_{n+1} and ζ_n is the 2D coordinate points at locations (n) and (n+1). The position of the ζ value can be seen at Figure 3-11.

Along the inner bank larger values are observed compared to the outer bank. In general there is a bound of amplified pressure RMS fluctuations between sections D0 and D180. This is the region where VI is coherent along the inner bank (see Fig.3-2). On the other hand, along the outer bank there are three regions where pressure RMS values are slightly larger which are around section D30, D60 and D135. Interestingly sections D60 and D135 are locations where vortex VO is initiated and dissipated (see Fig.3-2). Furthermore D30 is the section where vortex VM is initiated. Therefore it can be said that SOV cells are affecting the pressure RMS fluctuations on the bed and the banks.

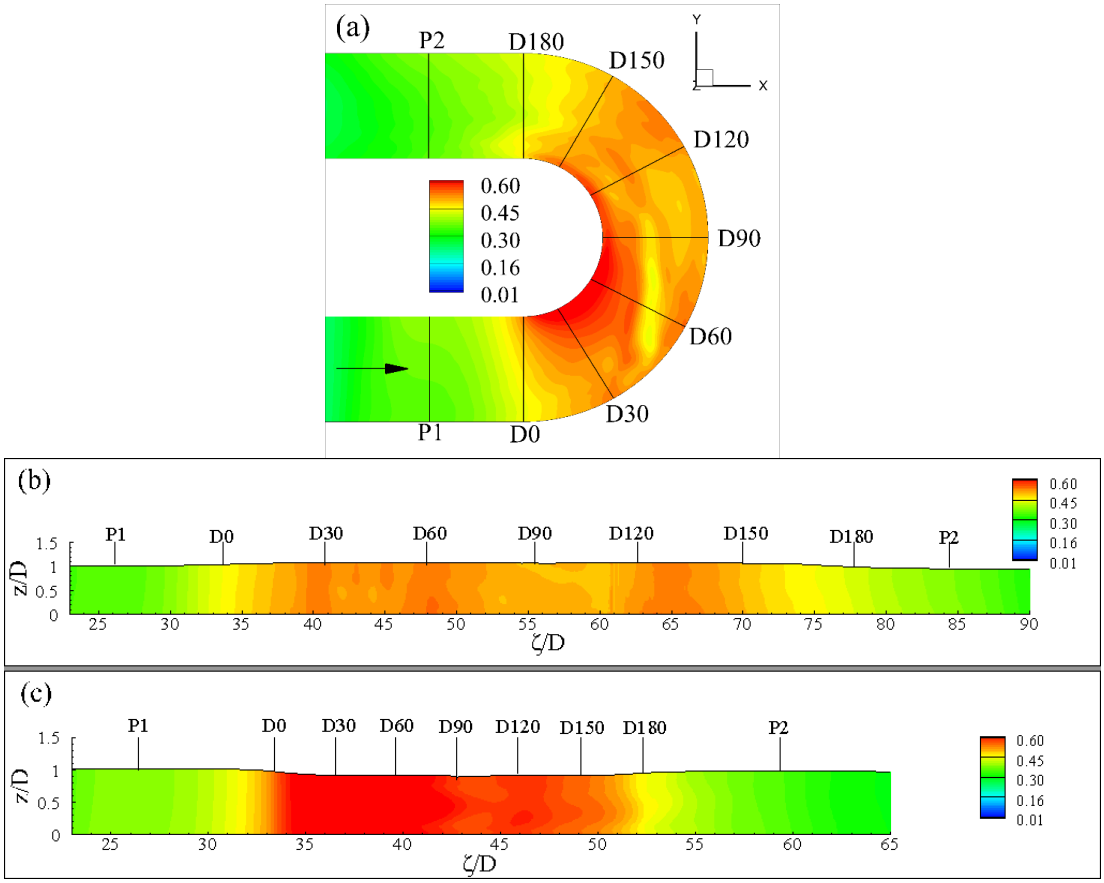

Figure 3-10 Distribution of the pressure RMS fluctuations, $\sqrt{p'p'}/\rho U^2$ a) on the channel bed, b) on the outer bank and c) on the inner bank

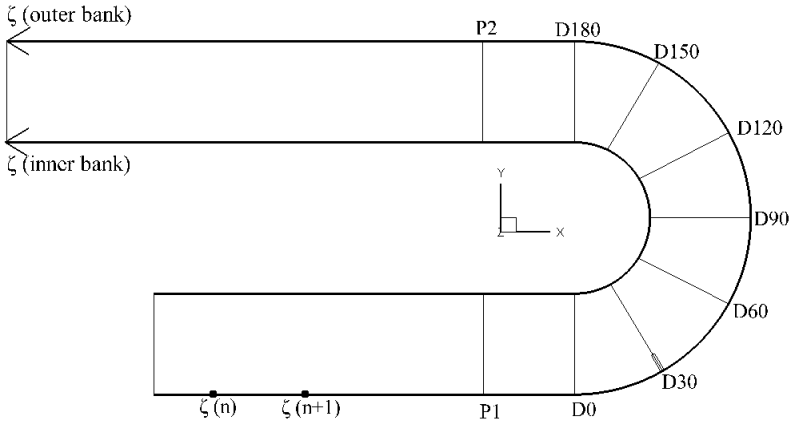

Figure 3-11 Position of the ζ value

Figure 3-12a shows the predicted shear stresses on the bed in the mean flow. Strong amplification of the bed shear stresses are predicted in the curved reach along the inner bank and channel centerline between sections D60 and D150 and at the straight reach after the curvature along the outer bank especially between sections D180 and P2. The regions of large bed shear stress roughly corresponds to regions where the streamwise velocities have higher values along the bed (Figure 3-7 (middle column)). Maximum non-dimensional bed shear stress value on the bed is 0.0533 which is observed between sections D90 and D120. There is a narrow bend along the outer bank where magnitude of the bed shear stress is small.

Large shear stress values along the outer bank is observed starting from section D180 in the streamwise direction throughout the whole flow depth. This amplification is related to the flow acceleration observed along the outer bank. Maximum non-dimensional shear stress value along the outer bank is 0.0452 which is observed after section D180.

Along the inner bank large shear stress values are observed between sections D0 and D180 parallel to the distribution observed along the bed. Different from the shear stress distribution along the outer bank, here the amplification is not observed through the whole flow depth except the small region downstream of section D0. The maximum non-dimensional bed shear stress is 0.00495 which occurs at the downstream of section D0.

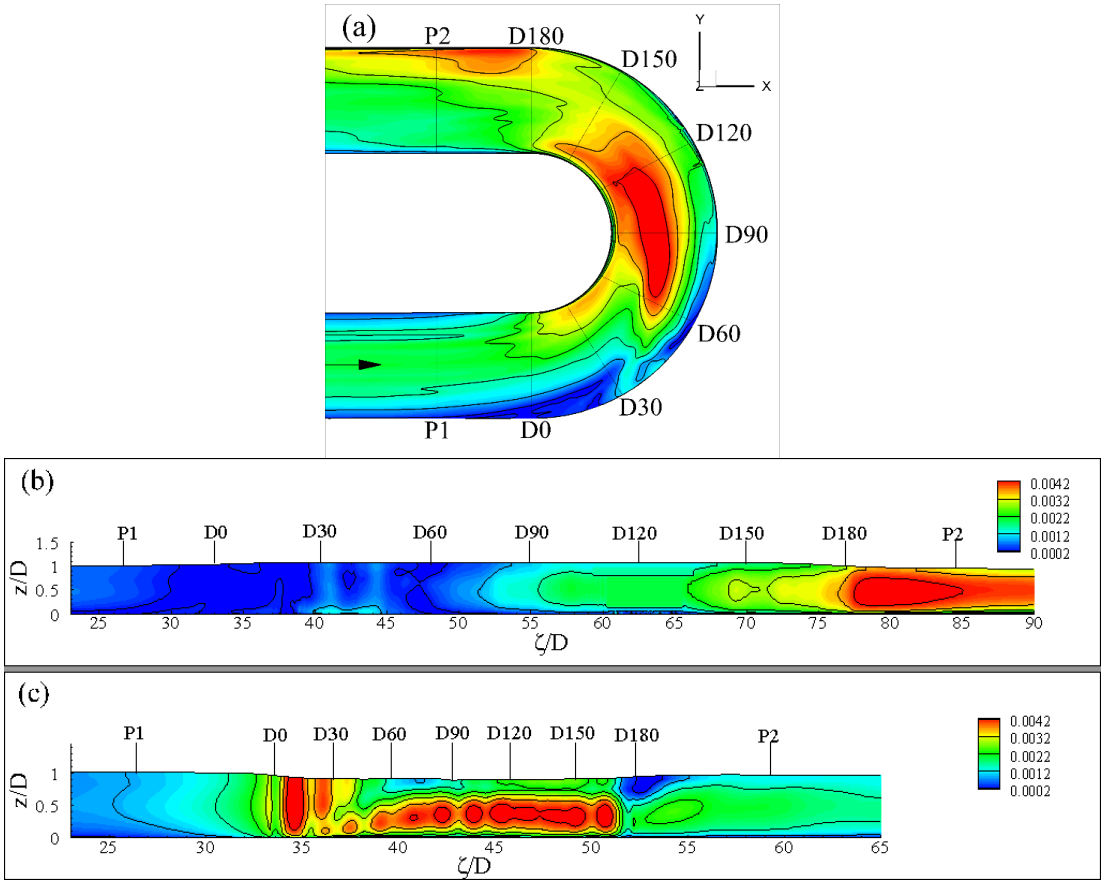

Figure 3-12 Non-dimensional shear stress distributions, $\tau_w/\rho V^2$, a) on the channel bed, b) on the outer bank, c) on the inner bank

CHAPTER 4

ANALYSIS OF THE MEAN FLOW STRUCTURES IN THE CURVED CHANNEL WITH SPUR DIKE

In this chapter investigation of the flow in the curved channel with a spur dike installed on the outer bank at section D30 is discussed. The spur dike installed on the outer bank has a length of 2D and a width of 0.33D. Different spur dike orientations are investigated where spur dike makes 45 degrees, 90 degrees and 135 degrees with the channel sidewall. These cases will named as S45, S90 and S135, respectively. Together with the case without the spur dike (NS), the four cases will be compared within this chapter.

4.1 Description of the Main Vortical Structures in the Mean Flow

Figures 4-1, 4-2 and 4-3 show the coherent structures visualized by Q criterion for the cases S45, S90 and S135, respectively. In all these three cases, similar to case NS, SOV cells VI and VM are present within the flow domain. Although vortex VI is similar in all the cases investigated, with the change in the orientation of the spur dike vortex VM shows considerable differences. With the inclusion of the spur dike in cases S45 and S90 the initiation point of VM migrates to section D0 on the outer bank (Fig. 4-1, Fig. 4-2). Compared to case NS, vortex VM loses its coherence at an earlier point between sections D60 and D90 in cases S45 and S90. On the other hand, in case S135 vortex VM is initiated close to the spur dike around section D30.

Compared to cases S45 and S90, in case S135 vortex VM is more coherent. It preserves its coherence up to section D120 where it is already very close to the inner bank and vortex VI. Presence of the spur dike brings some additional coherent structures within the flow domain. The coherent structures observed at the downstream of the spur dike are mostly related to the vortices that are shedding from the tip of the spur dike with the exception of VA which is a streamwise oriented vortex that forms close to the channel bed along the bank where the spur dike is attached (Koken & Constantinescu, 2008a). In all three cases with a spur dike vortex VA is present. Furthermore a horseshoe vortex, HV forms close to the channel bed around the spur dike tip in all three cases with a spur dike. An important observation made here is that the horseshoe vortex is very weak in cases S45 and S90 where it completely dissipates within the flow within a very short distance from the spur dike tip. Yet in case S135, HV is much more coherent where it preserves its coherence past section D60. One additional point that should be mentioned here is that with the presence of the secondary flow HV cannot persist its position close to the channel bed and moves towards the free surface within the streamwise direction (see Fig. 4-3 and Fig. 4-9). SOV cell VO which was observed in case NS is not present in cases S90 and S135. Only in case S45, VO is present which is less coherent compared to case NS (Fig. 4-1, Fig. 4-4, and Fig. 4-7).

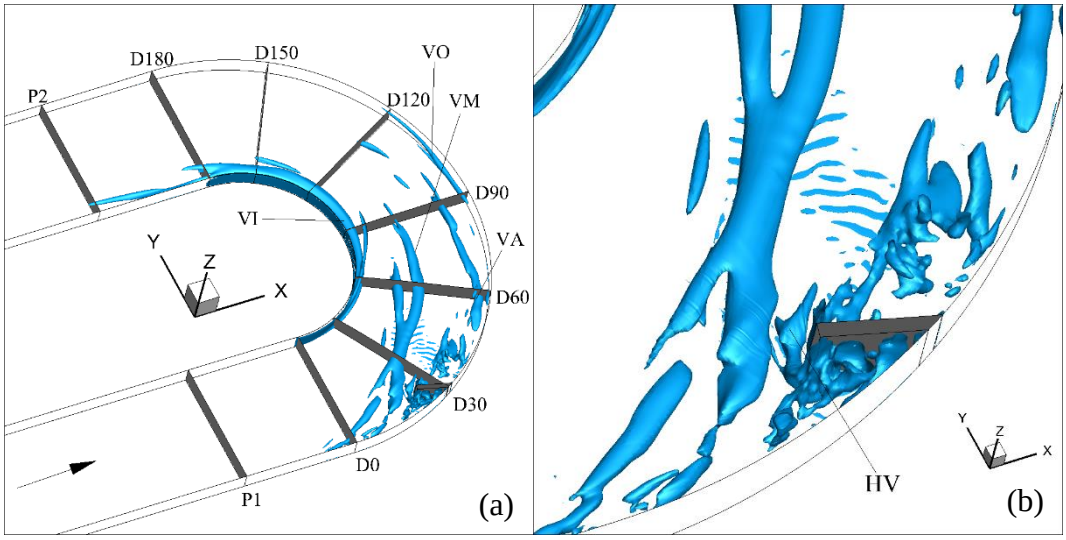

Figure 4-1 Three dimensional visualization of the vortical structure of the mean flow using the Q criterion a)at the whole channel, b)around the spur dike in case-S45

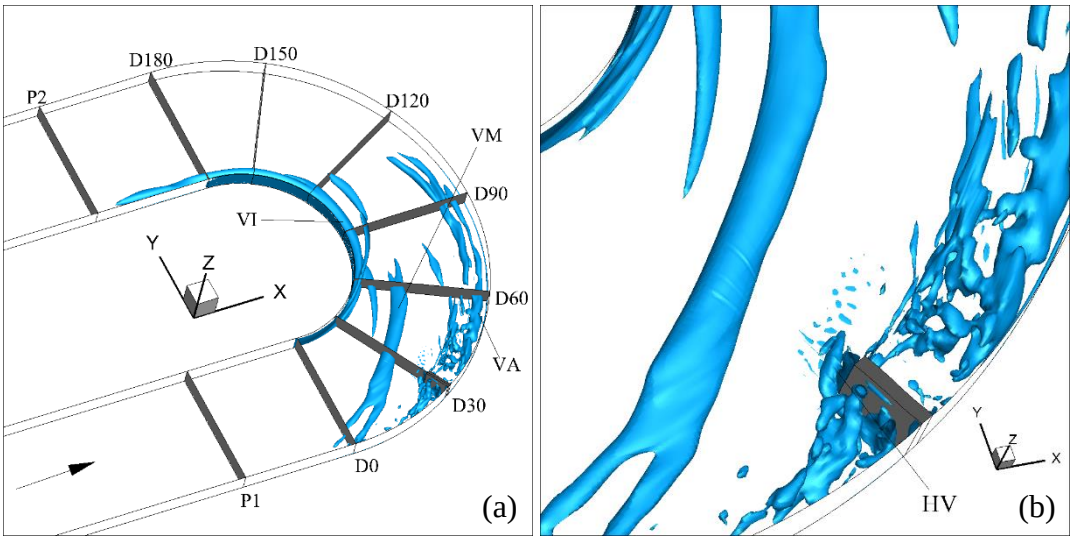

Figure 4-2 Three dimensional visualization of the vortical structure of the mean flow using the Q criterion a)at the whole channel, b)around the spur dike in case-S90

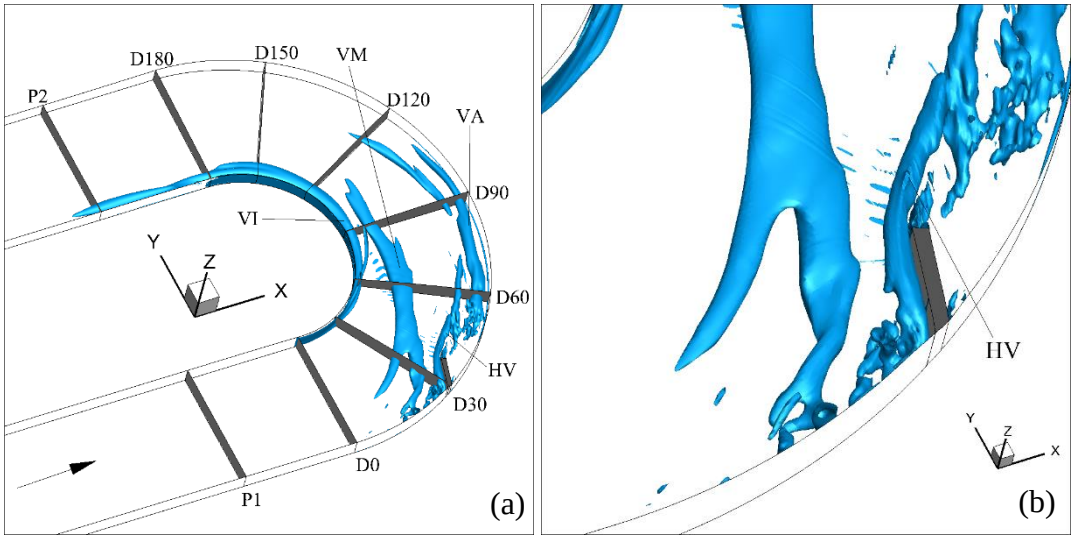

Figure 4-3 Three dimensional visualization of the vortical structure of the mean flow using the Q criterion a)at the whole channel, b)around the spur dike in case-S135

Figure 4-4, 4-5, and 4-6 show the mean streamline patterns on vertical sections for the cases S45, S90 and S135, respectively. One can clearly identify vortex VO in case S45, which is absent in cases S90 and S135. HV is only visible in case S45 at section D30 (Fig 4-4c) as in other cases this plane is not cutting the vortex in the direction perpendicular to its axis.

Figures 4-7, 4-8 and 4.9 shows the non-dimensional mean streamwise vorticity contours on the same vertical sections where streamline patterns were given. The largest streamwise vorticity contours is observed at section D90 for all the cases because the cross-stream circulation is the strongest here. It is almost impossible to distinguish the vortex VM ay any section whereas vortex VI can be identified at sections D60, D90 and D120. Vortex VO can clearly be identified along the outer bank D60 and D90 in case S45 (see Fig. 4-7). Horseshoe vortex close to the spur dike is also visible at section D30 of case S45. As discussed earlier, HV vortex gets away from the channel bed in case S135. The amplified patch of vorticity close to free surface at section D60 is associated with HV (see Fig. 4-9d).

Figure 4-10, 4-11, and 4-12 shows the non-dimensional streamwise velocity distributions at the same vertical sections for three cases observed. The highest streamwise velocity magnitudes is observed at the section D30 in the cases S45 and S90 and it is observed at the section D60 in the case-S135. Before the flow enters into the bend, high magnitude of the streamwise velocity is seen at the same position, i.e. at the the middle of the channel for the all cases. When the flow enters into the bend high core of the streamwise velocity moves towards to the inner bank for the all cases and at the sections D0, D30 and D60 seperation zone is clearly seen near the outer bank because of the negative velocity magnitudes.

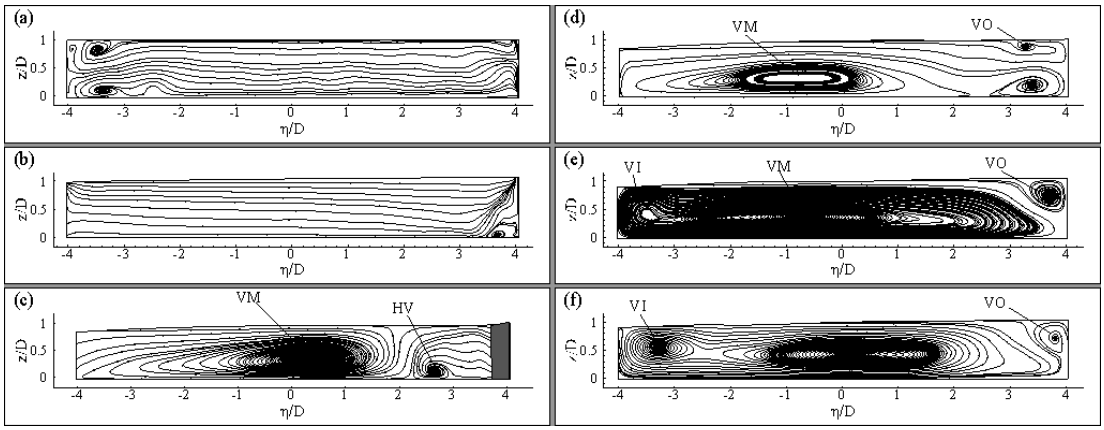

Figure 4-4 Streamline patterns at sections a)P1, b)D0, c)D30, d)D60, e)D90, and f)D120 in case-S45

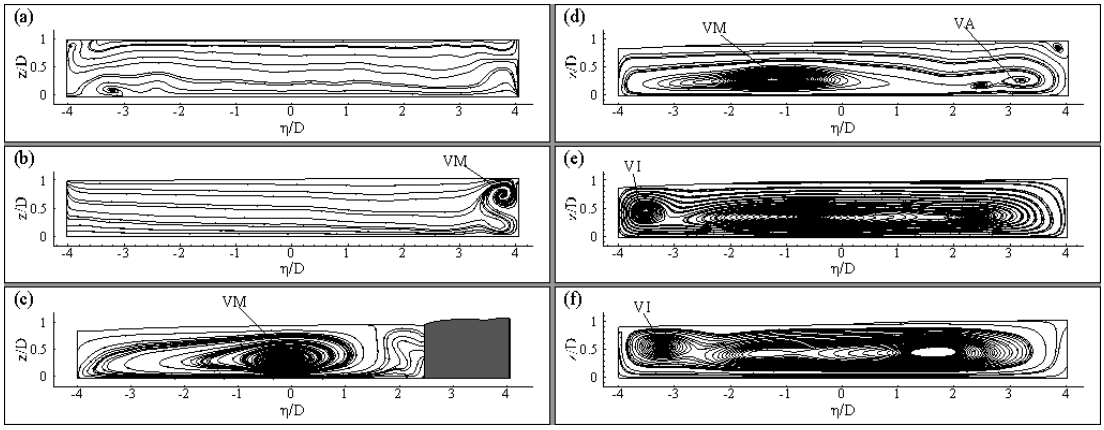

Figure 4-5 Streamline patterns at sections a)P1, b)D0, c)D30, d)D60, e)D90, and f)D120 in case-S90

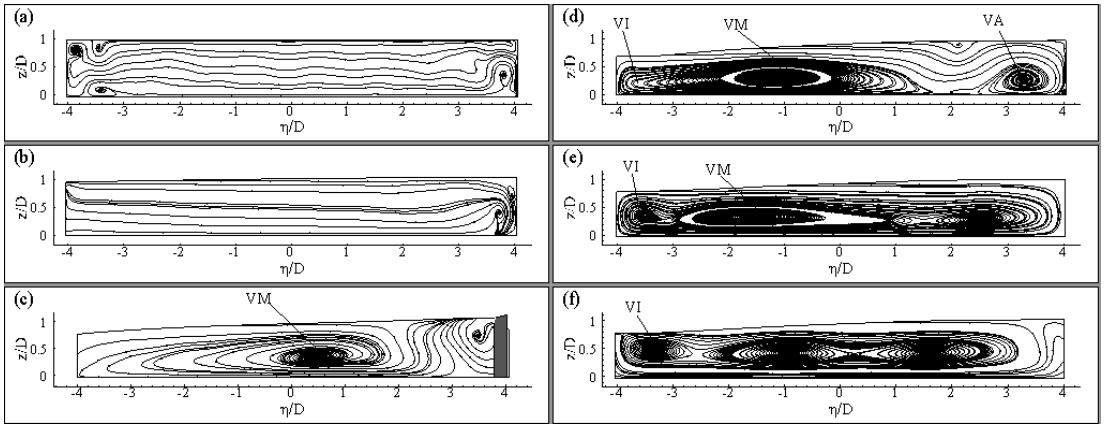

Figure 4-6 Streamline patterns at sections a)P1, b)D0, c)D30, d)D60, e)D90, and f)D120 in case-S135

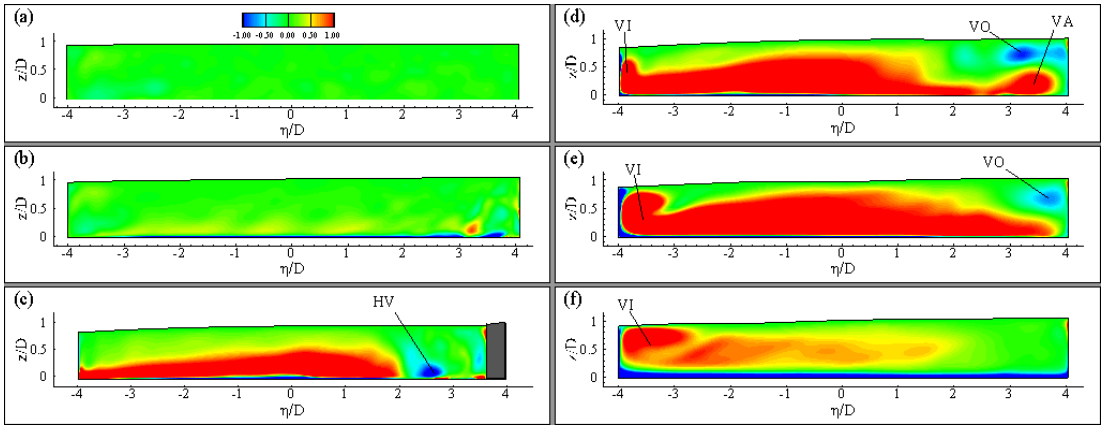

Figure 4-7 Non-dimensional mean streamwise vorticity distributions at sections a)P1, b)D0, c)D30, d)D60, e)D90, and f)D120 in case-S45

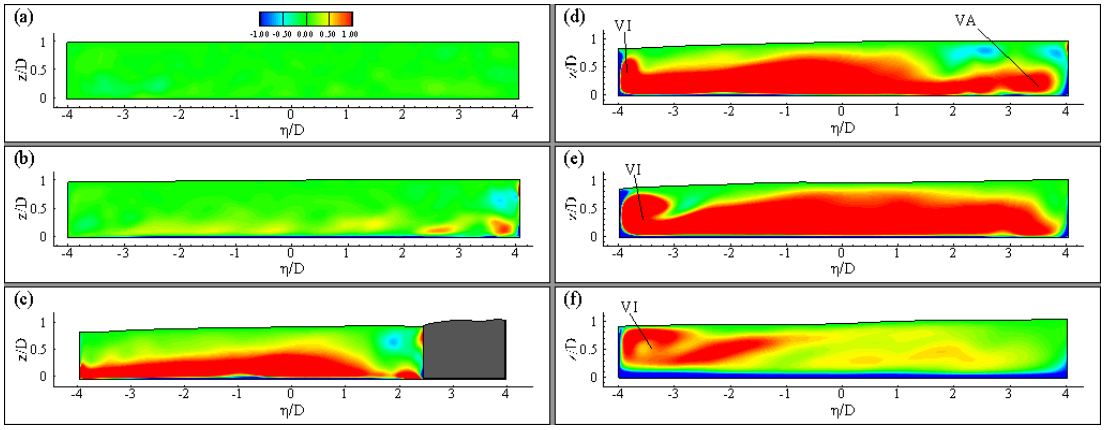

Figure 4-8 Non-dimensional mean streamwise vorticity distributions at sections a)P1, b)D0, c)D30, d)D60, e)D90, and f)D120 in case-S90

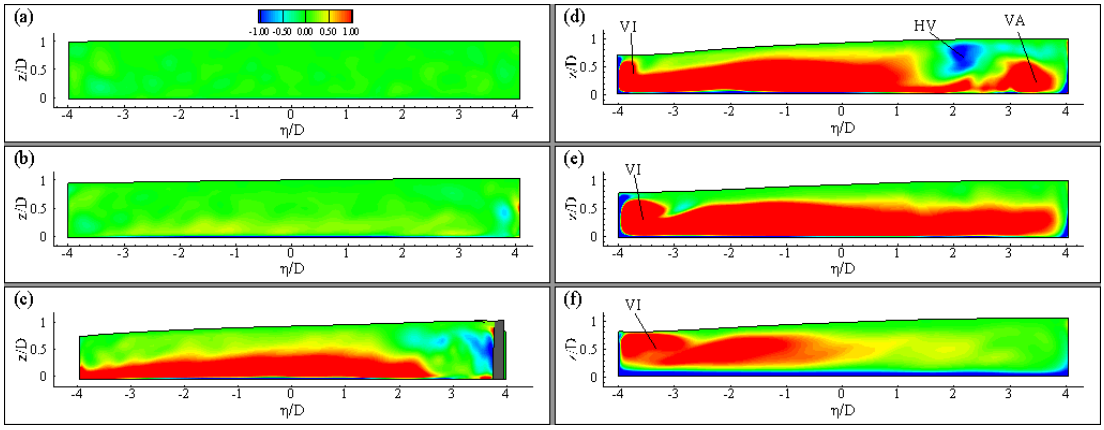

Figure 4-9 Non-dimensional mean streamwise vorticity distributions at sections a)P1, b)D0, c)D30, d)D60, e)D90, and f)D120 in case-S135

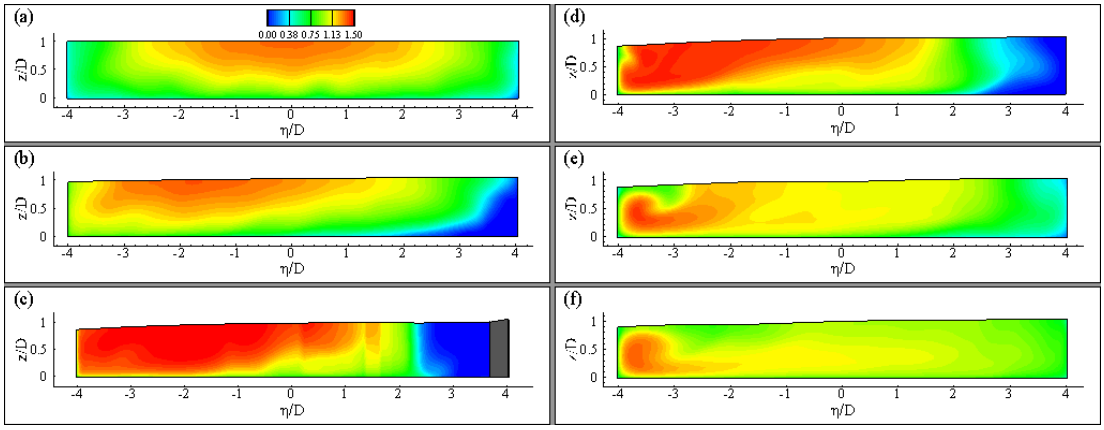

Figure 4-10 Non-dimensional mean streamwise velocity distributions at sections a)P1, b)D0, c)D30, d)D60, e)D90, and f)D120 in case-S45

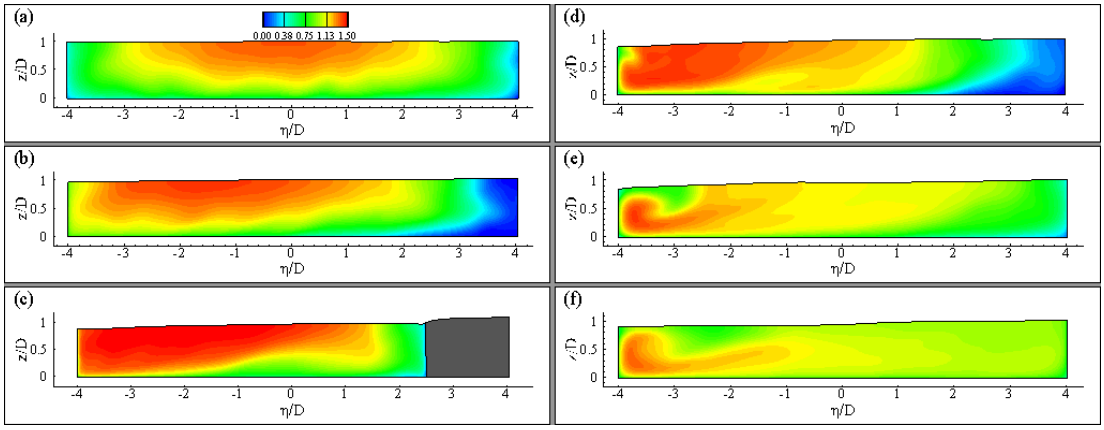

Figure 4-11 Non-dimensional mean streamwise velocity distributions at sections a)P1, b)D0, c)D30, d)D60, e)D90, and f)D120 in case-S90

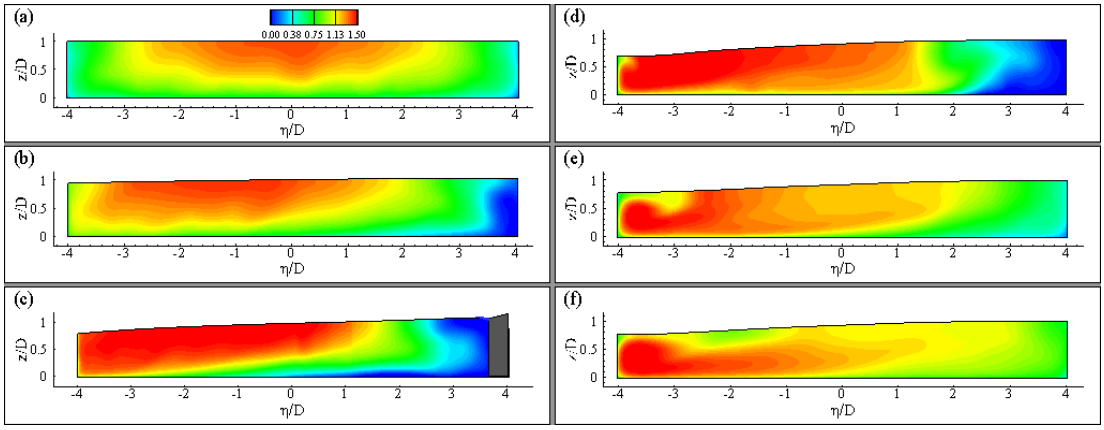

Figure 4-12 Non-dimensional mean streamwise velocity distributions at sections a)P1, b)D0, c)D30, d)D60, e)D90, and f)D120 in case-S135

4.2 Description of the Seperated Shear Layers and the Turbulence Kinetic Energy Distribution

Figures 4-13, 4-14, and 4-15 show the two dimensional streamline patterns, non-dimensional streamwise velocity distribution and out-of-plane vorticity contours on horizontal planes close to channel bed at mid-depth and close to free surface for cases S45, S90 and S135. Investigating the vertical vorticity contours on mid flow depth one can see the formation of an energetic shear layer which is initiated around

D60 on the inner bank. This shear layer forms as a result of the interface in between the low velocity flow close to the inner bank and high velocity flow away from the bank. It is present in all the three cases with the spur dike. Yet, this shear layer is only active within the top portion of the flow depth and disappears getting close to channel bed. Because of the decrease in flow depth along the inner bank on the horizontal plane close to the free surface there are some regions close to the inner bank where flow domain is not cut. This is why one cannot identify the initiation point of this shear layer using the plane close to the free surface.

In all three cases with the spur dike, there are two additional shear layers forming on the outer part of the channel which can be identified from the amplified vertical vorticity contours. These shear layers form as a result of the flow separation at the upstream and downstream of the spur dike (see the streamline patterns close to the spur dike, Fig. 4-13 and Fig. 4-15). One of these shear layers is initiated around section D0 on the outer bank whereas the other one is initiated from the tip of the spur dike.

Similar to case NS, in all the three cases with spur dike larger streamwise velocity magnitudes are observed close to the inner bank once flow enters into the bend. On the other hand, at the downstream of the bend larger streamwise velocity magnitudes are observed close to the outer bank.

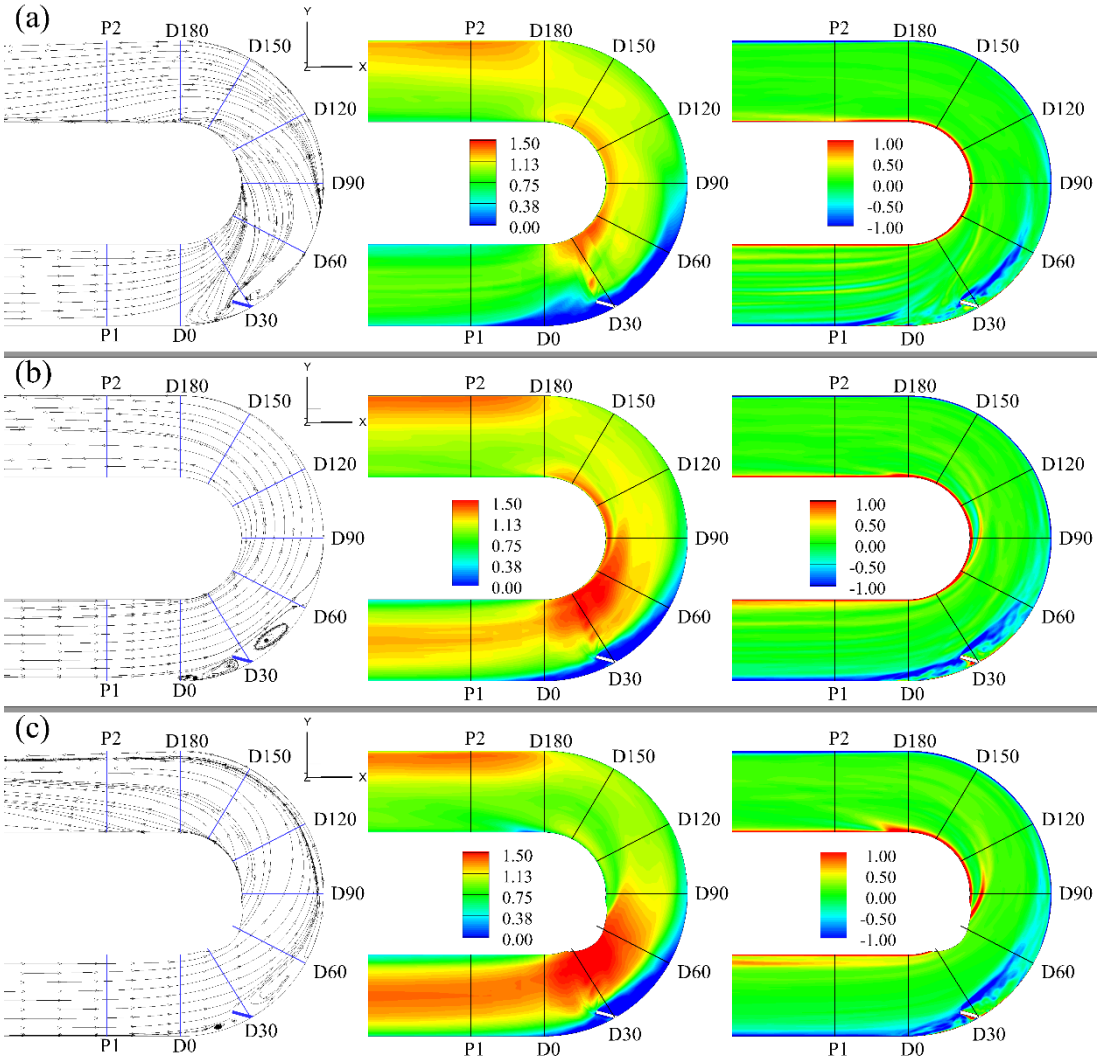

Figure 4-13 (a) Two dimensional streamline patterns (left), mean streamwise velocity contours, u_s/U (middle) and mean out-of plane vorticity contours, $\omega_z D/U$ (right) on horizontal planes at the level of a) 0.1D; b) 0.5D; c) 0.9D from the channel bed in case-S45

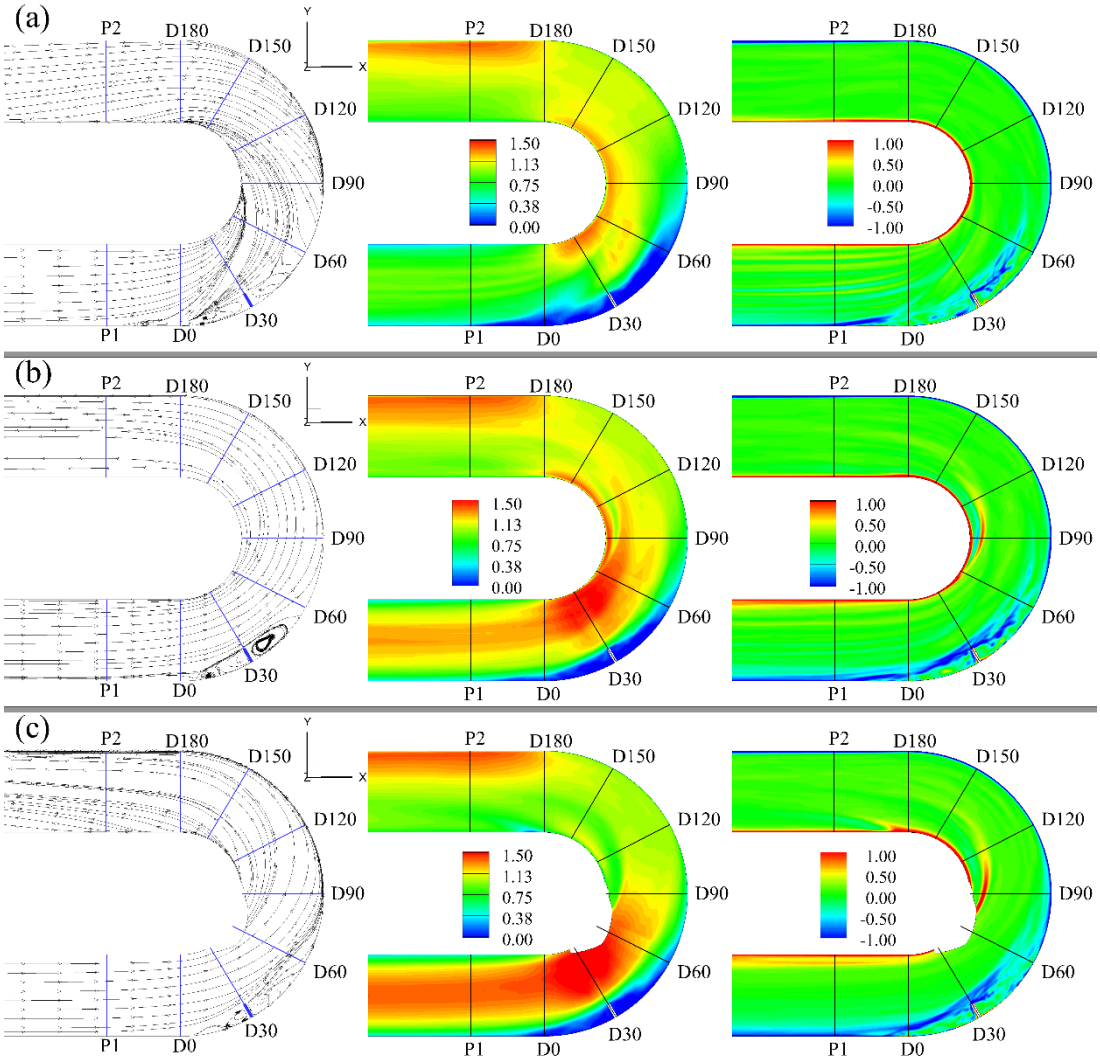

Figure 4-14 Two dimensional streamline patterns (left), mean streamwise velocity contours, u_s/U (middle) and mean out-of plane vorticity contours, $\omega_z D/U$ (right) on horizontal planes a at the level of a) 0.1D; b) 0.5D; c) 0.9D from the channel bed in case-S90

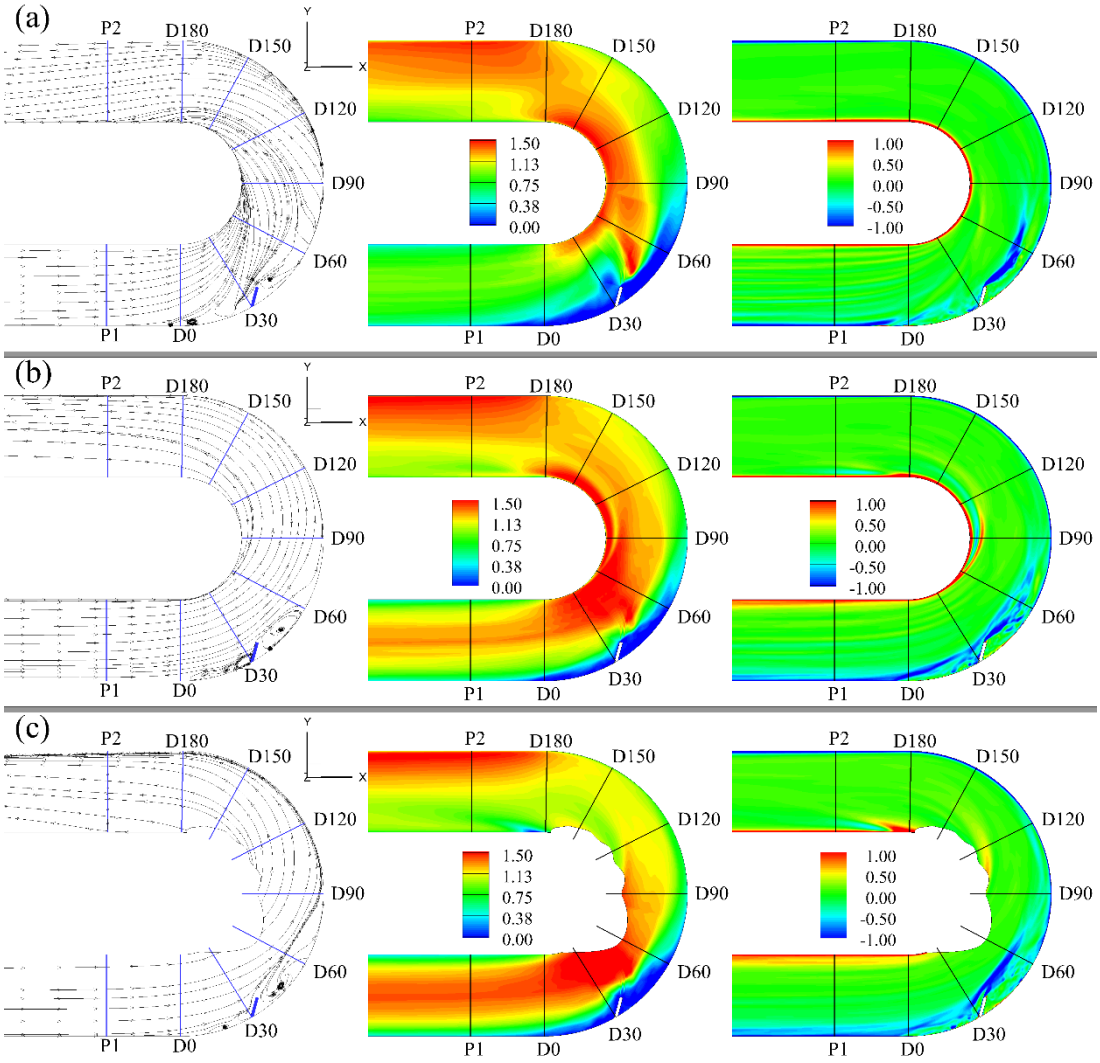

Figure 4-15 Two dimensional streamline patterns (left), mean streamwise velocity contours, u_s/U (middle) and mean out-of plane vorticity contours, $\omega_z D/U$ (right) on horizontal planes at the level of a) 0.1D; b) 0.5D; c) 0.9D from the channel bed in case-S135

In Figure 4-16 non-dimensional turbulent kinetic energy distributions on different horizontal planes for cases S45, S90 and S135 are shown. Unlike case NS, in the cases with the spur dike TKE values are amplified close to the tip of the spur dike and within its wake where lots of small scale coherent structures are populating the flow domain.

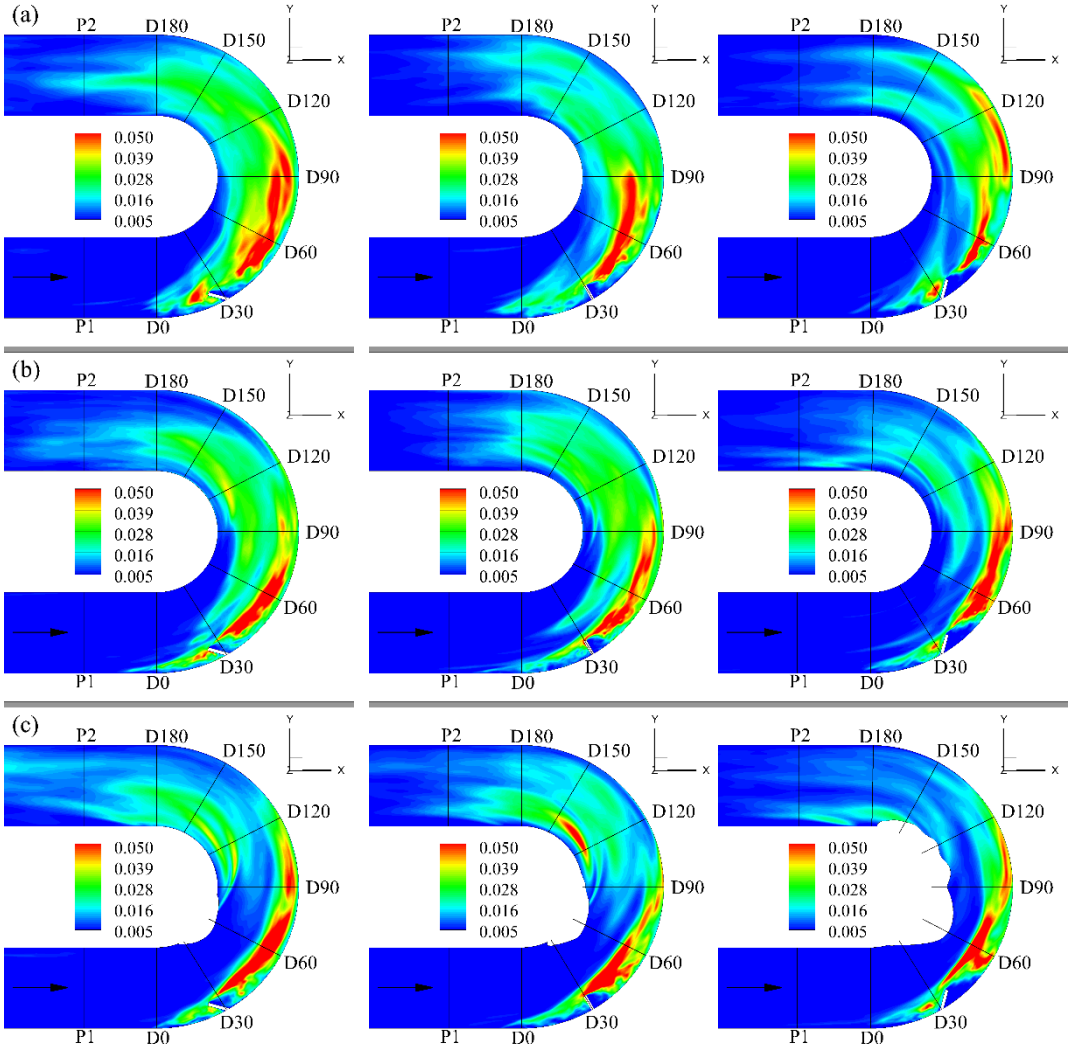

Figure 4-16 Distribution of turbulent kinetic energy at the level of a) 0.1D; b) 0.5D; c) 0.9D from the channel bed for the mean flow in the case-S45(left), S90(middle) and S135(right)

4.3 Pressure RMS Fluctuations and the Shear Stress Distributions

Pressure fluctuations on the bed is an important parameter related to the sediment entrainment in a channel flow. Figures 4-17, 4-18, and 4-19 show the pressure root-mean-square distributions on the bed, on the outer bank and on the inner bank for the cases S45, S90 and S135, respectively. At first glance, one can see the considerable

difference between the cases with and without the spur dike. In average for all the cases with the spur dike, the magnitude of the pressure RMS values decreased to 20% of the values observed in case NS along the whole channel cross section. This is an important indicator that inclusion of the spur dike in a curved channel helps reducing the pressure fluctuations on the bed and hence reduces the entrainment because of pressure fluctuations in an erodible channel. In case S45 (see Figure 4-17) the highest amplification of the pressure fluctuations on the bed is seen at the upstream and downstream of the spur dike between sections D30 and D60. The highest non-dimensional pressure RMS fluctuation value is 0.21, which is observed at section D45. Parallel with the amplification regions observed on the bed, along the outer bank just at the upstream of the spur dike and between sections D30 and D60 larger pressure RMS values are observed. On the inner bank there is not a considerable amplification. In case S90 (see Figure 4-18) large pressure RMS values are observed at the downstream of the spur dike between sections D30 and D60 close to the outer bank on the channel bed together with an amplification at section D45 on the outer bank. The highest non-dimensional pressure RMS fluctuation value is 0.18, which is observed at section D45. Lastly in case S135 (see Figure 4-19) high amplification of the pressure RMS fluctuation is seen upstream of the spur dike, and between the sections D60 and D150 close to the outer bank. The highest non-dimensional pressure RMS fluctuation value is 0.14, which is observed at section D90. The distributions of the outer bank and inner bank confirm the bed pressure RMS distributions. Among all cases, one can see that lower magnitudes of the pressure RMS fluctuation is seen in case S90.

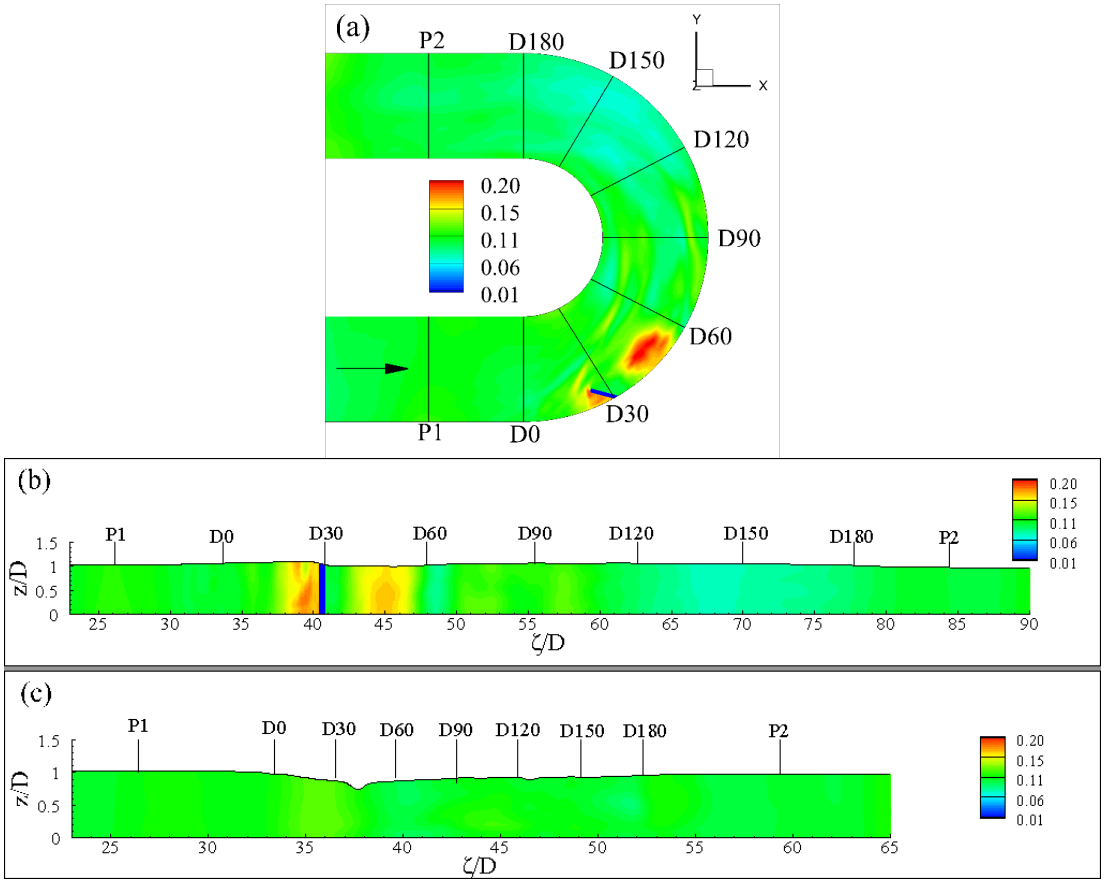

Figure 4-17 Distribution of the pressure RMS fluctuations, $\sqrt{p'p'}/\rho U^2$ a) on the channel bed, b) on the outer bank and c) on the inner bank in case-S45

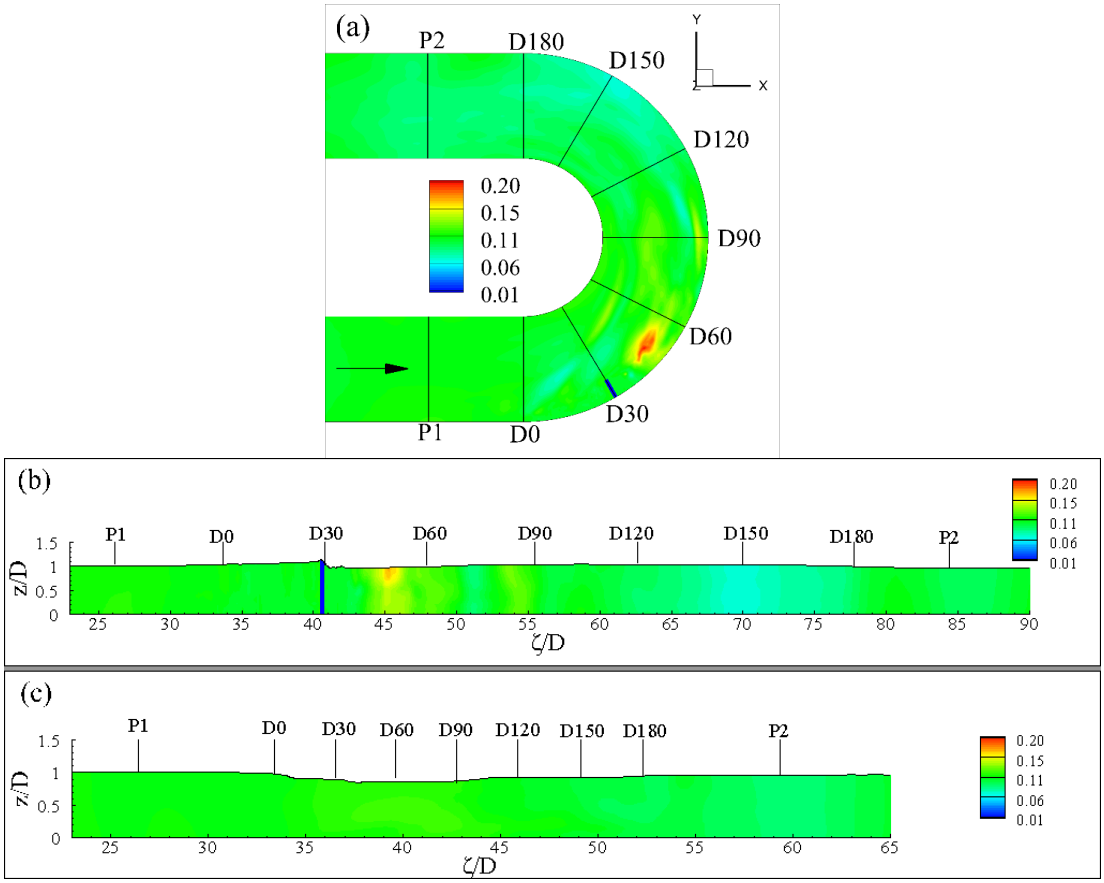

Figure 4-18 Distribution of the pressure RMS fluctuations, $\sqrt{p'p'}/\rho U^2$ a) on the channel bed, b) on the outer bank and c) on the inner bank in case-S90

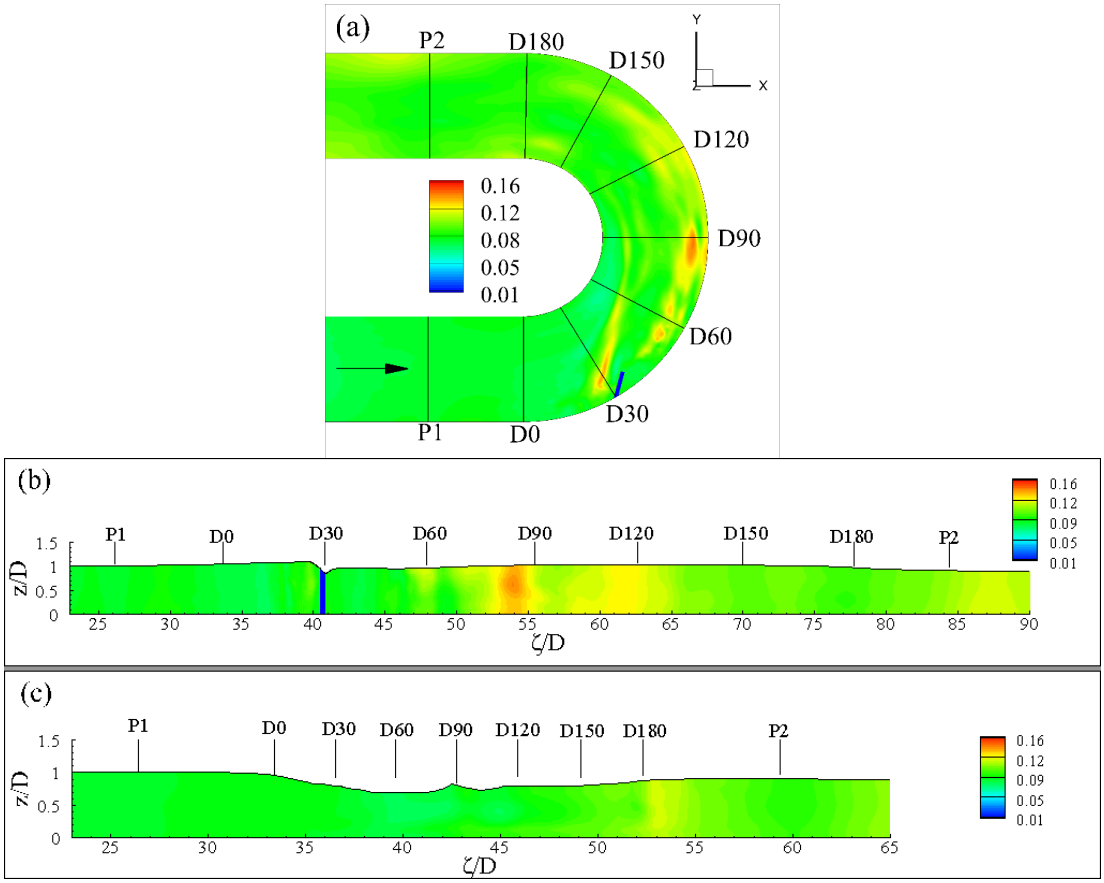

Figure 4-19 Distribution of the pressure RMS fluctuations, $\sqrt{p'p'}/\rho U^2$ a) on the channel bed, b) on the outer bank and c) on the inner bank in case-S135

Predicted shear stress distributions on the bed, on the outer bank and on the inner bank can be seen on Figures 4-20, 4-21, and 4-22 for cases S45, S90 and S135, respectively. Strong amplification on the bed shear stress values are predicted through the curvature between the inner bank and the middle of the channel and along the outer bank after the bend for all three cases. In case S45 it is observed that the area of high amplification region ($\tau_w/\rho V^2 > 0.004$) increased compared to case-NS. Maximum non-dimensional shear stress value on the bed is 0.0046 which is observed between sections D90 and D120 close to the inner bank. The peak value of the bed shear stress is 14% smaller than the case without the spur dike. In case S90 high amplification region ($\tau_w/\rho V^2 > 0.004$) is smaller in size which is observed around section D90 close to the inner bank. Maximum non-dimensional shear stress

value observed at this location is 0.0044. This peak value of the bed shear stress is found to be 18% smaller than the corresponding value in case NS. In case S135 one can clearly observe the overall increase in the shear stress on the whole bed. Compared to cases S45 and S90 the location of the maximum shear stress shifts in the downstream direction in case S135. Maximum non-dimensional shear stress value on the bed is 0.0051 which is observed between sections D120 and D150 close to the inner bank. The peak value of the bed shear stress is still 5% smaller than case NS. Predicted bed shear stress distribution is confirmed with the outer bank and the inner bank distributions in all cases. High amplification of non-dimensional shear stress distributions is seen through the curvature on the inner bank and after the curvature on the outer bank. From all cases, it can be said that in case S135 the amplification of the shear stress is higher and in case S90 it is smaller.

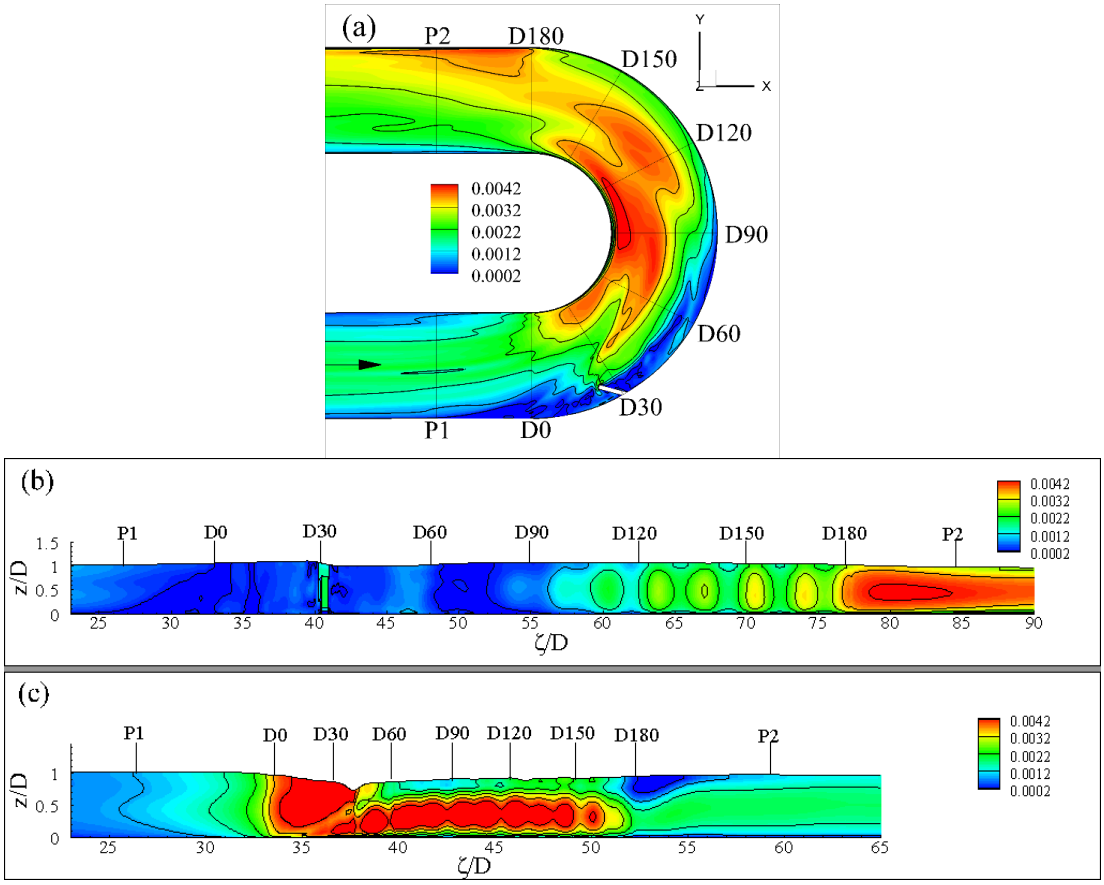

Figure 4-20 Non-dimensional shear stress distributions, $\tau_w/\rho V^2$, a) on the channel bed, b) on the outer bank, c) on the inner bank in case-S45

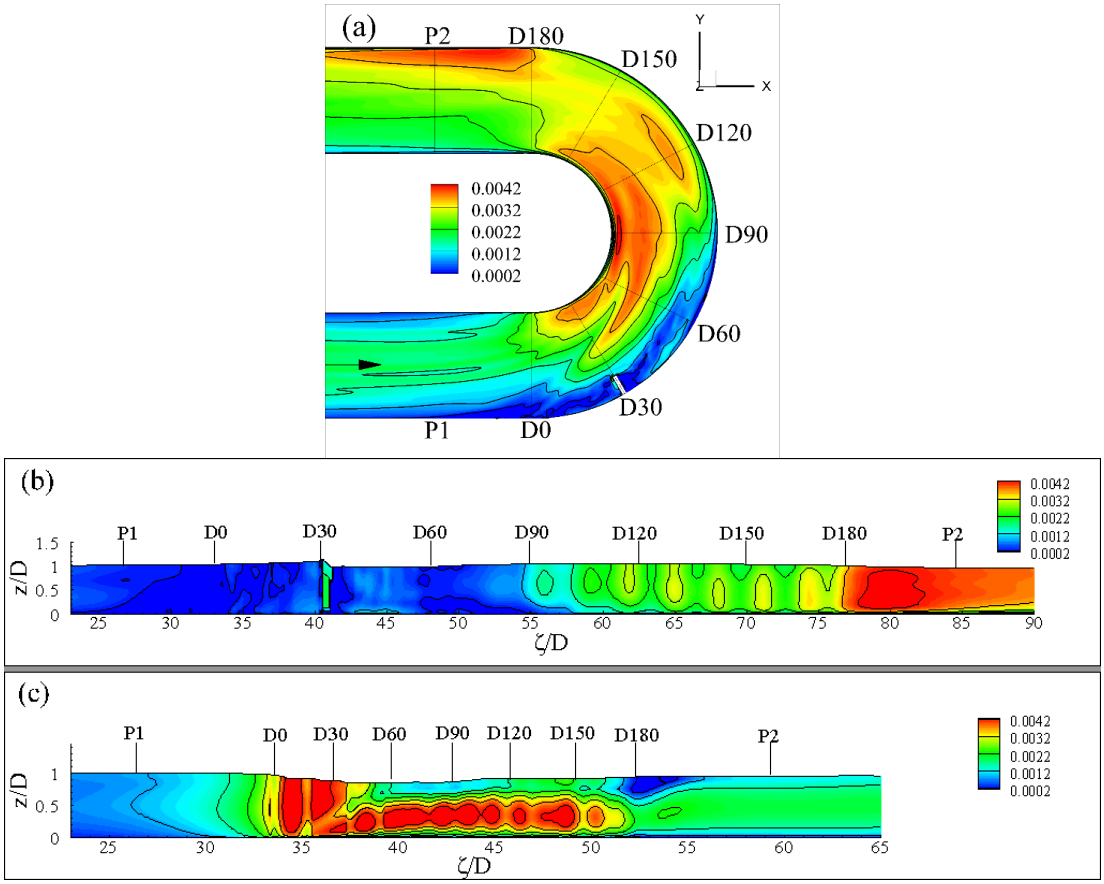

Figure 4-21 Non-dimensional shear stress distributions, $\tau_w/\rho V^2$, a) on the channel bed, b) on the outer bank, c) on the inner bank in case-S90

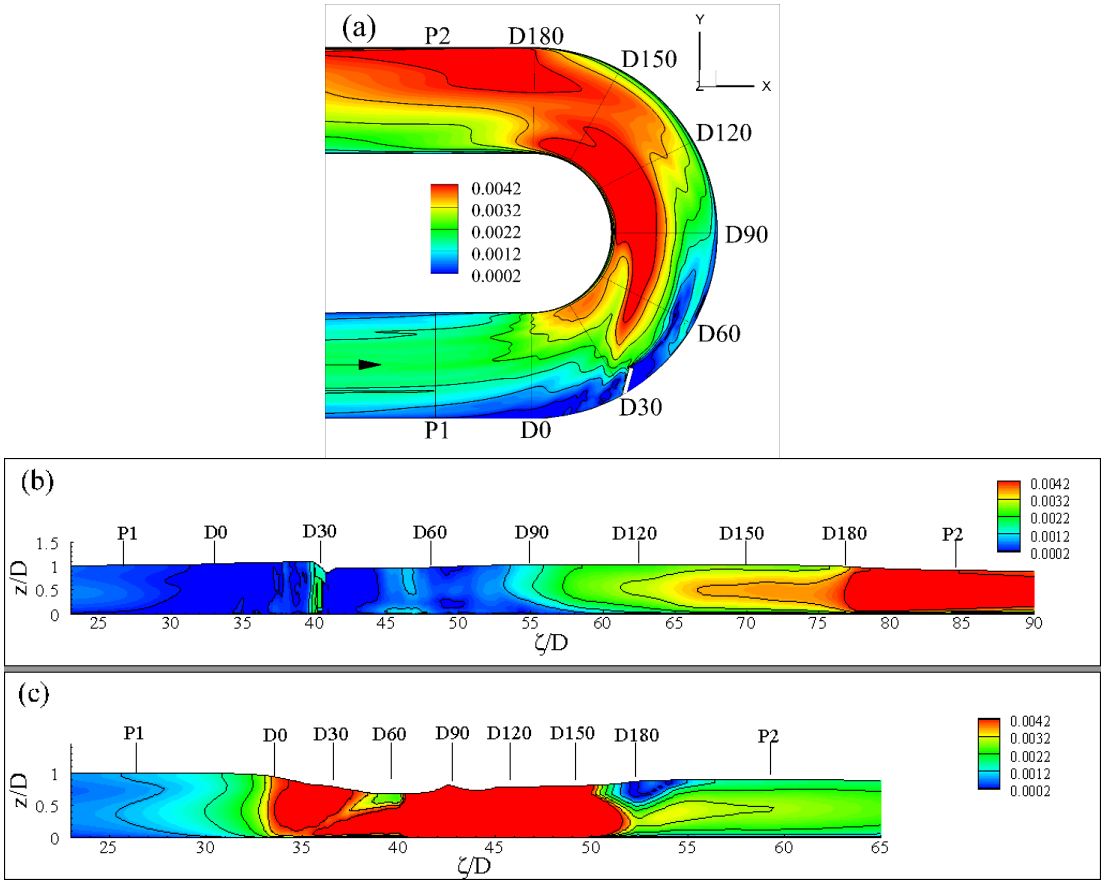

Figure 4-22 Non-dimensional shear stress distributions, $\tau_w/\rho V^2$, a) on the channel bed, b) on the outer bank, c) on the inner bank in case-S135

CHAPTER 5

CONCLUSIONS

5.1 Summary and Conclusions

Meandering channels create secondary flows because of the centrifugal forces that are acting on the flow due to the curvature. For large curvature values various coherent structures form within the curved flow section which contributes to scour process. Spur dike is constructed in order to prevent scouring that is formed due to the curvature of the meandering channel. However with the inclusion of a spur dike, the flow field becomes more complicated than it was. As flow approaches the spur dike flow seperates over the channel bed because of the adverse pressure gradients and this cause the formation of horseshoe vortex system around the spur dike.

In the present study, numerical investigation of flow is held in the 180° bend channel with and without the spur dike. Detached eddy simulation (DES) is used to simulate four cases within this investigation. Results of one case without a spur dike and three cases in which the spur dike exists with three different orientations are discussed. Obtained results are as follows:

- Several streamwise oriented vortices are formed within the flow domain in all four cases. Vortex VI which forms close to the inner bank and vortex VM which is in the middle of the channel are observed in all four cases. Although

VI is very similar to each other, the initiation point of VM close to the outer bank shifts in the upstream direction with the increase in the orientation angle of the spur dike. Furthermore, vortex VO, which forms close to the outer bank is seen only in cases NS and S45; however in case S45 it is less coherent than in case NS.

- Presence of the spur dike cause some additional coherent structures in the flow domain. In that respect the horseshoe vortex (HV) is seen around the spur dike close to the channel bed in all cases with the spur dike. In case S135 this HV is seen more coherent than the other cases.
- The highest streamwise vorticity value is seen at section D90 in all four cases because at this section cross-stream circulation is the strongest.
- The regions of higher streamwise velocity magnitudes are similar in all four cases. When the flow enters into the bend high core of the the streamwise velocity magnitudes moves towards the inner bank and throughout the curvature the highest values are observed close to the inner bank. After the curvature the highest values are seen along the outer bank.
- An energetic shear layer is formed between sections D60 and D120 close to the inner bank in all cases. This shear layer is formed because the streamline patterns cannot follow its original direction beacuse of the curvature and this results a slow moving fluid region near the inner bank. Actually this shear layer is between the high speed flow in the middle of the channel and slow moving fluid close to the inner bank. Furthermore in three cases with the spur dike two additional shear layers are seen. Flow seperation at the upstream and downstream of the spur dike cause the formation of these shear layers. One of them is initiated at section D0 and the other one is formed at the tip of the spur dike.
- With the inclusion of the spur dike, pressure RMS values on the bed and the banks decreases to approximately 20% of the values observed in case NS. This is a very important result because pressure fluctuation is an important parameter related to entrainment of the sediment on the bed in a channel

flow. That means that the presence of the spur dike may decrease the sediment entrainment. Among all four cases, in case S90 lower values of the pressure RMS fluctuations is seen.

- The regions of higher non-dimensionalized shear stress distributions are very similar in all cases. Large magnitudes of the shear stress distributions are observed along the inner bank through the curvature and at the straight reach after the curvature along the outer bank. However, the orientation of the spur dike considerably affects the shear stress distribution on the channel. In cases S45 and S90 the area that is prone to high shear stress values is small while in case S135 it is much larger. Therefore spur dikes oriented in the streamwise direction is not suggested to be used for scour protection in curved channels.
- S90 is the best orientation for scour reduction because of lower values of pressure RMS fluctuation and less magnitudes of the shear stress distribution.

5.2 Future Works

In this study, the influences of one spur dike and its orientations on flow domain are investigated numerically in 180 degrees channel bend. An experimental study can be done to verify this study in the future. Furthermore, serial spur dike configurations can be studied. Other than these aspects that are studied in this study, contamination risks between the spur dikes can be investigated.

REFERENCES

Azinfar, H. (2010). Flow Resistance and Associated Backwater Effect Due To Spur Dikes in Open Channels. *Thesis*.

Azinfar, H., & Kells, J. A. (2007). Backwater effect due to a single spur dike. *Canadian Journal of Civil Engineering*, *34*(1), 107–115. http://doi.org/Doi 10.1139/L06-117

Blanckaert, K. (2009). Saturation of curvature-induced secondary flow, energy losses, and turbulence in sharp open-channel bends: Laboratory experiments, analysis, and modeling. *Journal of Geophysical Research: Solid Earth*, *114*(3), 1–23. http://doi.org/10.1029/2008JF001137

Blanckaert, K. (2010). Topographic steering, flow recirculation, velocity redistribution, and bed topography in sharp meander bends. *Water Resources Research*, *46*(9), 1–23. http://doi.org/10.1029/2009WR008303

Blanckaert, K., & De Vriend, H. J. (2004). Secondary flow in sharp open-channel bends. *Journal of Fluid Mechanics*, *498*(2004), 353–380. http://doi.org/10.1017/S0022112003006979

Blanckaert, K., Duarte, A., Chen, Q., & Schleiss, A. J. (2012). Flow processes near smooth and rough (concave) outer banks in curved open channels. *Journal of Geophysical Research: Earth Surface*, *117*(4), 1–17. http://doi.org/10.1029/2012JF002414

Blanckaert, K., & Graf, W. H. (2001). Mean flow and turbulence in open-channel bend. *Journal of Hydraulic Engineering*, *127*(10), 835–847.

Breuer, M., Jovičić, N., & Mazaev, K. (2003). Comparison of DES, RANS and LES for the separated flow around a flat plate at high incidence. *International Journal for Numerical Methods in Fluids*, *41*(4), 357–388. http://doi.org/10.1002/fld.445

Constantinescu, G., Koken, M., & Zeng, J. (2011). The structure of turbulent flow in an open channel bend of strong curvature with deformed bed : Insight provided by detached eddy simulation. *Water Resources Research*, *47*, 1–17. http://doi.org/10.1029/2010WR010114

Constantinescu, G., & Squires, K. (2004). Numerical investigations of flow over a sphere in the subcritical and supercritical regimes. *Physics of Fluids*, *16*(5), 1449–1466. http://doi.org/10.1063/1.1688325

Dehghani A.A., Ghodsian M., Suzuki K., A. S. (2008). Local Scour Around Lateral Intakes in 180 Degree Curved Channel. In *16th IAHR-APD Congress and 3rd Symposium of IAHR-ISHS. Vol.III* (pp. 821–825). http://doi.org/10.1007/978-3-540-89465-0_144

GCSE Rivers Revision - The Middle Course. (n.d.). Retrieved August 21, 2017, from http://www.sln.org.uk/geography/schools/blythebridge/GCSERiversRevisionMC.htm

Koken, M. (2011). Coherent structures around isolated spur dikes at various approach flow angles. *Journal of Hydraulic Research*, *49*(6), 736–743. http://doi.org/10.1080/00221686.2011.616316

Koken, M., & Constantinescu, G. (2008a). An investigation of the flow and scour mechanisms around isolated spur dikes in a shallow open channel : 1 . Conditions corresponding to the initiation of the erosion and deposition process. *Water Resources Research*, *44*, 1–19. http://doi.org/10.1029/2007WR006489

Koken, M., & Constantinescu, G. (2008b). An investigation of the flow and scour mechanisms around isolated spur dikes in a shallow open channel : 2 . Conditions corresponding to the final stages of the erosion and deposition process. *Water Resources Research*, *44*, 1–16. http://doi.org/10.1029/2007WR006491

Koken, M., & Constantinescu, G. (2009). An investigation of the dynamics of coherent structures in a turbulent channel flow with a vertical sidewall obstruction. *Physics of Fluids*, *21*, 1–16. http://doi.org/10.1063/1.3207859

Koken, M., & Constantinescu, G. (2011). Flow and turbulence structure around a spur dike in a channel with a large scour hole. *Water Resources Research*, *47*, 1–19. http://doi.org/10.1029/2011WR010710

Koken, M., & Constantinescu, G. (2014). Flow and turbulence structure around abutments with sloped sidewalls. *Journal of Hydraulic Engineering*, 1–13. http://doi.org/10.1061/(ASCE)HY.1943-7900.0000876.

Koken, M., Constantinescu, G., & Blanckaert, K. (2013). Hydrodynamic processes , sediment erosion mechanisms , and Reynolds-number-induced scale effects in an open channel bend of strong curvature with flat bathymetry. *Journal of Geophysical Research: Earth Surface*, *118*, 1–17. http://doi.org/10.1002/2013JF002760

Koken, M., & Gogus, M. (2014). Effect of spur dike length on the horseshoe vortex system and the bed shear stress distribution. *Journal of Hydraulic Research*, *53*(2), 196–206. http://doi.org/10.1080/00221686.2014.967819

Shafaie, A., Ardeshir, A., Sadat-Helbar, S. M., & Saneie, M. (2008). The effect of minor spur dike on scouring at the first spur dike in the gravel bed. In *Fourth International Conference on Scour and Erosion* (pp. 196–200).

Shallow Flow Visualization around a Single Groyne. (2007). Retrieved August 24, 2017, from http://www.ifh.uni-karlsruhe.de/science/envflu/research/shallow-flows/project_single_groyne.htm

Strelets, M. (2001). Detached eddy simulation of nassively separated flows. In *Aiaa 2001-0879* (pp. 1–18). http://doi.org/10.2514/6.2001-879